MINERAL RECYCLING IN THE ACTIVE SYSTEM OF STROMBOLI VOLCANO: AN OLD STORY OF ABOUT 2.5 ka AS INFERRED BY *IN-SITU* Sr-ISOTOPE AND TRACE-ELEMENT DATA IN THE 2002-2003 PRODUCTS

Francalanci L.[1,2,✉], Nardini I.[1], Avanzinelli R.[1], Chertkoff D.G.[3], Tiepolo M.[4], Davidson J.P.[3], Vannucci R.[4]

1- Dipartimento di Scienze della Terra, Università degli Studi di Firenze, via La Pira, 4, I-50121, Firenze, Italy.
2- C.N.R.-I.G.G., Sezione di Firenze, via La Pira, 4, I-50121, Firenze, Italy.
3- Department of Earth Sciences, University of Durham Science laboratories, South Road, Durham DH1 3LE, UK.
4- Dipartimento d Scienze della Terra, Università degli Studi di Pavia, 27100, Pavia, Italy.

✉ *Corresponding author, e-mail: lorella.francalanci@unifi.it*

Key words: microanalyses, isotopic microdrilling, Sr-isotope disequilibria, mineral recycling, Stromboli.

Abstract

In-situ Sr-isotope data by microdrilling technique, coupled with major and trace element analyses, have been performed on plagioclase and clinopyroxene of seven samples collected during the 2002-2003 eruptive crisis at Stromboli volcano (Aeolian islands, Italy). During this period, the persistent moderate explosive activity characterising this volcano and mainly ejecting scoria bombs, lapilli and ash, was broken by an effusive events lasting about seven months (28 December 2002 – 22 July 2003). Furthermore, a more violent explosion (paroxysm), also erupting light pumice occurred on 5 April 2003. A volatile-poor and highly-porphyritic magma (HP-magma), with about 50 vol% of olivine, clinopyroxene and plagioclase, is represented by scoria and lavas, whereas a volatile-rich magma with very low phenocryst contents (LP-magma; usually < 5 vol%) of olivine and clinopyroxene, is erupted as pumice. LP-magma is slightly less evolved, but has a distinct composition of groundmass and lower Sr-isotope ratios (0.70610 for LP-magma of 5-April paroxysm) than HP-magma.

Although rock textures, mineral compositions and major element contents of whole-rocks are practically constant along the course of the effusive event and incompatible trace element abundances only slightly decrease in lavas after the 5-April paroxysm, Sr-isotope ratios more significantly decrease passing from 0.70616 to 0.70615 in whole-rocks and from 0.70616 to 0.70613 in groundmasses. Micro-Sr isotope data show the presence of zoned minerals in strong

isotope disequilibrium, as previously found in products erupted in 1984, 1985 and 1996 AD, with $^{87}Sr/^{86}Sr$ values generally decreasing from cores to rims of minerals. Only some outer-rims are found in equilibrium with the host groundmass.

The internal mineral zones with high Sr-isotope ratios (0.70665-0.70618) are considered to represent "antecrysts", crystallised during the previous activity and recycled in the present-day system. The presence of antecrysts, whose abundance increases from the onset to the end lavas (estimated from about 12% to 20% of whole-rock), seems to be a constant characteristic of this system and, together with the interaction between HP- and LP-magmas, allows maintaining the typical present-day steady state conditions. The highest $^{87}Sr/^{86}Sr$ values of the antecrysts, combined with their trace element data, indicate they are recycled since the opening shoshonitic activity of the Recent Period, which occurred at about 2.5 ka ago. Although only one low Sr-isotope crystal zone is drilled in the internal part of a clinopyroxene (0.70597), the presence of these zones, grown in equilibrium with LP-magmas, is inferred by several calculations in proportions 30/70 between low/high Sr-isotope crystal zones.

These data allow understanding the dynamics of the present-day plumbing system of Stromboli at intermediate pressure (about 2-3 km depth), where we propose that an HP-magma reservoir is directly interconnected at the bottom with a cumulus crystal much reservoir. Efficient mixing between HP- and LP-magmas can occur in this reservoir, due to more similar rheological characteristics of the two magmas than in the conduit, where further crystallisation driven by degassing occurs leading the mineral compositions and the rock textures to reach those typical of HP-products. Antecrysts (and possibly melts) re-enter in the HP-magma reservoir both from the bottom, recycled by ascending LP-magmas crossing the crystal mush, and from the top, recycled by descending degassed and dense HP-magma, residual of the periodic Strombolian explosions at the surface. A considerable amount of LP-magma arrived in the shallow reservoir before the onset of the 2002-2003 lava flows and mixed with the interstitial melt of the HP-magma triggering, some months later, the effusive eruption. New LP-magma was left in the reservoir after the 5-April paroxysm, starting to produce an effect at the surface only in the $^{87}Sr/^{86}Sr$ values of the lava groundmass erupted from May onwards, and carrying further antecrysts into the end lava system. Finally, we try some calculations on the involved magma volumes, estimating at about 0.002 km^3 the conduit volume, corresponding to about 25% of the total lava volume, which in turn may be a proportion of 20% of the inferred HP-magma reservoir volume. The total volume of LP-magma input during 2002-2003 is also tentatively estimated to be similar to the magma volume erupted in the effusive event.

1. Introduction

Mineral/liquid elemental and isotopic disequilibria are often found in volcanic rocks and are useful for revealing pre-eruptive magmatic processes. Indeed, bulk rocks frequently represent a mechanical mixture of various phases with possible different origin (e.g., Davidson and Tepley III, 1997; Wolff et al., 1999; Tepley and Davidson, 2003; Davidson et al., 2007 and reference therein). Mineral phases preserve the history of changing physical and chemical conditions during their growth, thus recording more information on processes occurring during the magma ascent to the surface than the whole-rock. Accordingly, *in-situ* mineral determinations of $^{87}Sr/^{86}Sr$ values, associated with major and trace element analyses on core-rim traverses, give us the opportunity to recognize the timescales during which magmas arise from their source to their emplacement by eruptions. Furthermore, these information help to better understand the configurations of the volcanic plumbing systems. Both laser ablation (e.g., Davidson et al., 2001; Ramos et al., 2004) and microdrilling techniques (e.g., Tepley III et al., 1999, 2000, Perini et al., 2003) have been used for *in-situ* analyses on phenocrysts and associated glasses.

This paper reports the results of *in-situ* Sr-isotope analyses performed in the products (lavas, scoria and pumice) erupted during the 2002-2003 period at Stromboli volcano (Aeolian islands, Italy), and obtained by the microdrilling method.

The present-day volcanic activity of Stromboli generally consists of mild explosions, at intervals of 3-5 per hour, which eject black scoria bombs, lapilli and ash around the craters. This normal "Strombolian" activity is sometimes interrupted by lava flows and more violent explosions (paroxysms of different scale) also erupting around a larger area small volumes of light coloured pumice, together with scoria and blocks (Bertagnini et al., 1999, 2008; Rosi et al., 2000). The 2002-2003 eruptive crisis, characterised by one of the most voluminous lava flow of Stromboli in the past two centuries, was the most dangerous volcanic crisis occurred in Italy after the 1944 eruption of Vesuvius. The crisis had its peak on December 30, two days after the onset of the lava flow, when the eastern part of the Sciara del Fuoco collapsed, producing a tsunami that devastated the NE coast of the island. Furthermore, after about three months from the beginning of the lava effusion, on 5 April 2003, a paroxysmal eruption occurred at the summit craters. The lava flow continued for about seven months and it was periodically sampled mainly from the active channels (Landi et al., 2006, 2008).

Several recent papers have allowed improving the knowledge of the behaviour of the present-day magmatic system of Stromboli (e.g., Allard et al., 1994, 2010; Francalanci et al., 1999, 2004, 2005; Métrich et al., 2001, 2005, 2010; Landi et al., 2004; Bertagnini et al., 1999, 2008 and reference therein), but little is still known on the detailed processes controlling the change from the typical

mild explosive activity to the more vigorous paroxysms and lava flow eruptions. In particular, previous works focussed on Sr isotope ratios and on micro-Sr isotope analyses have pointed out the importance of these data in understanding the dynamics of the present-day volcanic system of Stromboli, and the presence of complex mineral/liquid Sr-isotope disequilibria in products erupted between 1984 and 1996 AD (Francalanci et al., 1999, 2005, 2008). The latter led to propose the possible existence of a cumulus crystal mush zone sited at intermediate depth.

The present paper combines *in-situ* Sr-isotope and major and trace element data of minerals and glassy groundmasses for several samples erupted during the seven months of 2002-2003 crisis, in order to better understand the isotope disequilibrium processes and to shed lights on the crystal recycling mechanisms and the characteristics of the crystal mush. These results are also useful to improve our understanding of the timescales of pre-eruptive magmatic processes controlling the style of the present-day Strombolian activity.

2. General background

Stromboli island is the northernmost stratovolcano of the Aeolian arc, Southern Tyrrhenian Sea, which is located on 20 km thick continental crust (Morelli et al., 1975) (Fig.1). The volcano has an elevation of 924 meters above sea level (m. a.s.l.) and continues for 2,000 m b.s.l. The oldest subaerial rocks (204 ± 25 ka) form the Strombolicchio neck, located NE of Stromboli island and belonging to the same submarine edifice, whereas the island rose from the sea about 100 ka ago (Gillot and Keller, 1993). The volcanic history of Stromboli was characterised by six main volcano-building periods (from the oldest to the youngest: Paleostromboli I, II, III, Vancori, Neostromboli and Recent; Fig.1) alternated to volcano-collapsed periods (Francalanci et al., 1993; Hornig-Kjarsgaard et al., 1993). Among the eight edifice collapses, the youngest ones led to the formation of the Sciara del Fuoco depression in its present form, on the NW flank of the volcano (Pasquarè et al., 1993; Kokelaar and Romagnoli, 1995; Tibaldi, 2001).

During the last 200 ka, Stromboli outpoured magmas ranging from calc-alkaline (mainly basaltic-andesites), to potassic-alkaline (potassic leucite-bearing trachybasalts and shoshonites), through high-K calc-alkaline (high-K basalts and andesites) and shoshonitic (shoshonitic basalts to trachytes) (Francalanci et al., 1988; 1989; 1993; Hornig-Kjarsgaard et al., 1993). The variable composition of the erupted magmas also characterises the different periods of activity. Strombolicchio neck and the products of the Paleostromboli II period (~ 60 ka) are calc-alkaline (Fig. 1). Pyroclastic deposits and lavas erupted during the Paleostromboli I (~ 85 ka) and III (~ 35 ka) periods have mainly high-K calc-alkaline compositions, whereas the activity of the Vancori

period (~ 26–13 ka) was mostly characterised by shoshonitic lava flows. Potassic-alkaline lava flows were erupted during the Neostromboli period (~ 13-6 ka) from central and eccentric vents, which were mainly located in the north-western part of the volcano. Effusive and Strombolian activity, erupting shoshonitic (e.g., "Pizzo-Sopra-la-Fossa tuff" and present-day products) and high-K basalts (e.g., "San-Bartolo lavas"), mainly characterise the Recent period of activity (younger than ~2.5 ka) (Fig. 1) (Hornig-Kjarsgaard et al., 1993; Gillot and Keller, 1993; Speranza et al., 2008, Di Salvo, 2010).

The variation of magma composition from calc-alkaline to potassic lavas is associated with a general increase in incompatible trace element contents and Sr isotope ratios, whereas Nd isotope ratios generally decrease. Thus, due to the correlation between magma composition and period of activity, the products from each period are practically characterised by specific Sr-Nd isotope data (Fig. 1). In particular, Sr isotope ratios are lowest in the calc-alkaline rocks (Strombolicchio and Paleostromboli II periods) and highest in the potassic rocks (Neostromboli period), whereas they decrease with time in the last 6 ka from Neostromboli period onwards (Francalanci et al., 1988; 1989; 1993; 1999; 2004).

3. The present-day Strombolian activity

The present-day Strombolian activity, which begun between the third and seventh century (Rosi et al., 2000), takes place from several vents in a crater terrace, situated at 750 m a.s.l. on top of the Sciara del Fuoco depression (Fig. 1). The "normal" mildly explosive activity ejects fountains of blocks, black scoria bombs, lapilli and ash at variable intervals of about 3-5 events per hour. Although each crater is characterised by a different explosive dynamics, infrasonic, thermal and seismic data indicates that the feeding system is shallow (about 500 m. a.s.l.) and common to all the vents. The activity also consists of a persistent bursting of small gas bubbles (one burst every 1-2 s), which occur at only one vent at once (puffing). This overpressurized style of degassing releases more gas (~100 t/d) than "normal" Strombolian explosions (~35 t/d) (Ripepe et al., 2002, 2008 and reference therein).

The normal explosive activity is sometimes interrupted by lavas flowing into the Sciara del Fuoco and lasting from <3 days to 11 months (Barberi et al., 1993; Capaldi et al., 1978). Recent notable effusive events occurred from December 1985 to April 1986 (De Fino et al., 1988), in the 2002-2003 period (Landi et al., 2006, 2008; Spampinato et al., 2008) and from February 27th to April 2nd 2007 (Landi et al., 2009).

The present-day activity is also characterised by more violent explosions ("major explosions") than the usual ones, which occur with a frequency of about 1–3 events per year (Barberi et al., 1993; Bertagnini et al., 1999). The major explosions eject meter-sized scoriaceous bombs and blocks up to the Pizzo Sopra la Fossa peak and lapilli and ash up to the coastal zones. When coarse blocks and bombs also reach the coasts, these violent eruptions are referred to as "paroxysms". The last paroxysms occurred on 5 April 2003 and 15 March 2007, when the lava flows were still active. Tsunamis are also generally associated to paroxysmal eruptions and landslides along the Sciara del Fuoco scar. The last tsunami occurred on 30 December 2002, triggered by landslides related to the lava effusion (Bonaccorso et al., 2003).

A volatile-poor highly-porphyritic magma (hereafter the "HP-magma") is erupted as black scoria bombs and lapilli by the normal mildly explosive activity and by lava flow effusions. Instead, during major explosions and paroxysms, the most voluminous juvenile component still consists of black scoria similar in composition to those of the normal activity (HP-magma), but a second component consists of a highly-vesiculate light pumice, representing a volatile-rich magma with low phenocryst content (hereafter the "LP-magma") (Bonaccorso et al., 1996; Francalanci et al., 1999, 2004; Bertagnini et al., 1999; Métrich et al., 2001). Black scoria and light pumices are usually mingled at different scales.

3.1. Petrochemical background

Black scoria and lavas (HP-magma) have seriate textures with high phenocryst content (ca. 45-60 vol% of phenocrysts and microphenocrysts) and a glassy to microcrystalline groundmass. The most abundant mineral phase is represented by plagioclase (on average ≈ 35 vol. %), followed by clinopyroxene (on average ≈ 15 vol. %) and olivine (on average ≈ 5 vol. %). Microphenocrysts mostly consist of plagioclase and some olivine (Francalanci et al., 2004, 2005; Landi et al., 2004; Bertagnini et al., 2008).

Clinopyroxene is the largest phase (0.5-5 mm, sometimes around 1 cm in length) and ranges from augite to diopside, with Mg# [molar $Mg^{2+}/(Mg^{2+}+Fe^{2+})$] mainly between 0.70 and 0.91. Zoning can be normal or oscillatory, also including this wide compositional variation usually in a single large crystal. Outer rims are always augitic (Mg# around 0.74-0.78), in equilibrium with the groundmass composition, whereas cores, augitic to diopsidic, are often partially resorbed.

Olivine from black scoria and lavas commonly ranges between 0.2-3 mm in size, being the second largest mineral phase. It varies in composition from Fo_{64} to Fo_{74} (average of Fo_{70}) and is usually in equilibrium with the groundmass. When present, zoning is weak, normal or reverse.

The plagioclase phenocrysts are between 0.1-2.5 mm in length and show a large compositional range (An_{60-87}). The largest plagioclase crystals usually have resorbed cores and complex zoning in the rims, with sieved textures found either in the cores or in repeated growth zones. The outer rims, however, are usually around An_{65}, being the composition of plagioclase in equilibrium with the groundmass composition. Glomeroporphyritic aggregates of olivine and clinopyroxene, with interstitial plagioclase, are also common in the HP-products (Francalanci et al., 2004, 2005; Landi et al., 2004; Bertagnini et al., 2008). The compositional range of olivine, clinopyroxene and plagioclase in scoria and lavas has remained nearly the same since the beginning of the 20th century (Francalanci et al., 2004) and, probably, since the beginning of the present-day Strombolian activity (Bertagnini et al., 2008).

Light pumice (LP-magma) has a weakly porphyritic seriate texture (< 10 vol % of crystals, usually ≈ 5 vol %) with a glassy groundmass. Minerals consist of olivine, clinopyroxene and plagioclase, with variable proportions in different samples (Rosi et al., 2000; Métrich et al., 2001; Francalanci et al., 2004). Euhedral crystals, in equilibrium with the glassy groundmass, are usually small (<0.5 mm), whereas the largest minerals crystallised from the HP-magmas (e.g., crystals in compositional equilibrium with and often surrounded by a more evolved glass than the pumice glassy groundmass) and were included into the LP-magma by syn-eruptive mingling processes (Francalanci et al., 2004).

Olivine crystals of the pumice generally have a large compositional range (Fo_{68-86}) and sometimes, the phenocrysts are strongly reversely zoned: cores with compositions similar to those of the olivine in the HP-products and rims and microphenocrysts with the highest Fo contents. The latter olivine composition is that in equilibrium with the groundmass composition. Homogeneous, and normally or reversely zoned MgO-rich olivine (Fo_{88-91}) are also found in pumices of the large-scale paroxysms, often associated with Cr-spinel (Cr# 64-67, Mg#59-67) (Bertagnini et al., 2008). Clinopyroxene of the pumice shows the same compositional range as found in the clinopyroxene of the HP-products with Mg# between 0.69-0.91. Phenocrysts are often oscillatory zoned with the outer rims usually having high Mg# values (0.84-0.91), which are similar to those of the microphenocrysts and are the clinopyroxene composition in equilibrium with the groundmass composition. Plagioclase shows a large variation in An content (An_{60-90}), but microphenocrysts and the rims of phenocrysts, which are considered to be in equilibrium with the LP groundmass, usually have An > 80%. Single phenocrysts display strong (e.g., An_{65-85}) complex reverse or oscillatory zoning. Cores are often partially resorbed and have variable An contents (Métrich et al., 2001; Francalanci et al., 2004).

The scoria, lavas and pumice erupted since the onset of the Strombolian activity, are high-K and shoshonitic basalts. LP-magmas are slightly less evolved than the HP-magmas, with lower silica and K_2O contents (about 1 wt% and 0.5 wt% of difference, respectively). HP-magmas have slightly higher incompatible trace element contents, except for Sr, and slightly lower MgO, Co, Ni, V, and Sc abundances than LP-magmas (Rosi et al., 2000; Francalanci et al., 2004, 2005; Bertagnini et al., 2008).

The matrix glass compositions of LP- and HP-products are quite distinct. Pumice glasses are shoshonitic basalts, whereas scoria and lava glasses have more evolved compositions with SiO_2 and K_2O contents between 51-53 and 3.5-5.2 wt%, respectively. Compositional gaps in MgO (between 3.8 and 5.5 wt%), CaO (7.8-10 wt%), Al_2O_3 (16-17 wt%) and FeO (8.6-9.2 wt%) are present between the pumice glasses and the scoria and lava glasses.

Sr isotope ratios of HP-magmas remained nearly constant since the beginning of the 20th century to around 1980 A.D. (0.70626 ±2, 2σ) . After 1980, $^{87}Sr/^{86}Sr$ smoothly decreases to a value of 0.70615 (Francalanci et al., 1999, 2004, 2005) of the present-days. LP-magmas have significantly lower Sr isotope ratios than HP-magmas, with $^{87}Sr/^{86}Sr \approx 0.70610$. Nd isotope ratios of scoria, lavas and pumice show a slight inverse correlation with Sr isotopes, but their variation is very low (0.51256 ±1; Francalanci et al., 1999, 2004).

An *in-situ* major and trace element and Sr isotope microanalysis study was previously performed in four samples representing the products of different types of eruption from the present-day activity of Stromboli (Francalanci et al., 2005). The samples were collected from the 1985-86 lava flows, from the scoria bombs of the 1984 "normal" activity and from the scoria and coeval pumices of the 1996 major explosion. Large and comparable Sr isotope disequilibrium has been found in plagioclase and clinopyroxene. HP-magma crystals have cores with either high $^{87}Sr/^{86}Sr$ (≈ 0.70635) or low $^{87}Sr/^{86}Sr$ (≈ 0.70614-0.70608). In the former case, the cores are usually resorbed. Low $^{87}Sr/^{86}Sr$ values, similar to those found in some cores, are also found in the outer cores grown around the more Sr radiogenic cores. Mineral rims and groundmasses generally have similar and intermediate $^{87}Sr/^{86}Sr$ (≈ 0.70628-0.70613). LP-magma crystals have growth zones with similar groups of $^{87}Sr/^{86}Sr$ values, but the lowest values are present in the mineral rims and glassy groundmasses.

4. The 2002-2003 eruptive crisis

The 2002-2003 eruptive crisis consisted of several phenomena ranging from the contemporaneous lava outpouring from multiple vents (28 December 2002 - 22 July 2003), a

paroxysm on 5 April 2003 while lava emission was still in progress, and a tsunami generated by the collapse of the Sciara del Fuoco flank into the sea.

The effusion started on 28 December 2002 from vents opened at the foot of the NE cone (≈ 600 a.s.l., Fig. 1) (Landi et al., 2006, 2008; Spampinato et al., 2008). Specifically, the eruption began with a short-lived mild explosive episode from a lateral vent, generating a hot avalanche deposit at the base of the Sciara del Fuoco, which was soon followed by the overflow of lava from the NE summit crater rim. The lava overflow lasted less than one hour and led to the emplacement of an exceptionally fluid flow descending the northeast slope of the Sciara del Fuoco down to the sea. Soon after, less fluid lava was outpoured from a vent opened in the NE portion of the Sciara del Fuoco at 600 m a.s.l. (Fig. 1). After the onset of the effusive activity, the draining of lava from lateral vents led to a drop of magma level in the central conduit, to the collapse of the craters and the accumulation of cool debris within their bottom, and to the cessation of the mild explosive Strombolian activity.

During the first two days the effusion was characterised by relatively high lava discharge rate (Marsella et al., 2008) from different vents and by contemporaneous gravity movements in the Sciara del Fuoco which, on 30 December, culminated with two, four minutes apart, tsunamigenic collapses of the eastern, both submarine and subaerial, sector of the Sciara del Fuoco. The cumulative volume of the landslides has been estimated around 53.5×10^6 m^3 (Bonaccorso et al., 2003; Tommasi et al., 2004, 2005). Soon after the landslide, effusive activity concentrated in vents located at 550 m elevation within the scar left by the landslide. During January momentary stops of the lava flow were soon followed by lava outpouring again from the vents at 600 m. a.s.l. at the foot of the NE cone ("Pianoro" place; Fig. 1). On 5 April 2003 a paroxysmal eruption occurred in the summit craters and in the lava field. It was the most violent event of the last 50 years leading to: a) a fallout deposit of bombs, lithic blocks and ash all over the upper part of the volcano, b) a fallout deposit of light pumice in the southern flanks of the cone down to the sea, c) the launch of meter-sized ballistic blocks along the volcano flanks and on the Ginostra village, d) the accumulation of a thick pyroclastic flow deposit, rich in mingled scoria-pumice bombs, onto the active lava field in the Pianoro. The effusive activity stopped for a couple of hours and then resumed from three vents at the edge of the Pianoro (Rosi et al., 2006; Francalanci et al., 2008; Pistolesi et al., 2008; Harris et al., 2008).

Since middle April 2003, degassing and spattering activity started from the lava vents on Pianoro resulting in the rapid growth of two hornitos, attaining an elevation above the lava field of 25 m in July. Intensification of explosive activity in the central craters also occurred. On July, lava output rate decreased and ended on 22 July. The waning phase of the lava output was accompanied

with a rapid rise of the magma in the central conduit and the full resumption of the Strombolian activity in all the craters (Puglisi et al., 2005; Ripepe et al., 2005; Landi et al., 2006, 2008). The total lava volume was estimated at $12.5x10^6$ m^3, with an average effusion rate of about $0.7m^3/s$ (Marsella et al., 2008).

5. Sampling and analytical methods

29 lava samples were collected during the whole effusive eruption (Table 1 of Landi et al., 2006). Some rocks derive from the beginning of the effusive activity, collected in the summit area near the eruptive fissures and along the Sciara del Fuoco. From January onward, periodic samplings of the lava were performed, every 10-15 days, from the active lava channel in the lava field at 550-600 m a.s.l., generally quenching the samples in water. Scoria and pumice erupted from the 5 April paroxysm, were also collected. Because they were strictly mingled together, it was only possible to obtain scoria-uncontaminated pumice samples, but not viceversa.

Modal analyses and major element data of whole rocks, matrix glasses and mineral phases from the collected samples of the 2002-2003 eruptive crisis, together with trace element and Sr-Nd isotope analyses of whole rocks, were reported and discussed in Landi et al. (2006, 2008) and Francalanci et al. (2008). In the present paper, from a representative number of samples of the 2002-2003 eruptive crisis, we report and discuss i) core-rim micro-Sr isotope data of selected plagioclase and clinopyroxene by microdrilling technique, ii) Sr isotope ratios of glassy groundmasses (both micro-drilled and separated by handpicking), iii) Sr isotope ratios of some separated single crystals of olivine and clinopyroxene, iv) major and trace element data of the selected micro-drilled minerals (Tables 1-3, Tables ESM-1, ESM-2). In order to perform microdrilling of minerals, the most zoned plagioclase and clinopyroxene crystals were chosen from each thin section of the selected samples.

5.1. EMPA-WDS analyses

Major element analyses of plagioclase, clinopyroxene and glassy groundmass were performed by the Jeol JXA 8600 superprobe at the CNR-IGG in Florence. Operating conditions were 15kV accelerating voltage, 10nA beam current (monitored on a Faraday cup) and variable counting times for major and minor elements. The applied matrix correction method is according to Bence and Albee (1968). In order to avoid or minimise alkali loss, we used a defocused beam (10μm) and a lower counting time for Na, measuring both Na and K at the beginning of each analyses. Detailed description of analytical procedure with precision and accuracy of measurements are provided by

Vaggelli et al. (1999). Natural silicate minerals and glasses were mostly used as primary and secondary standards, whereas a repeatedly analysed polished section (STR09/96e, glass composition reported in Francalanci et al., 2004) from the present-day activity of Stromboli was used for further checking of precision and for allowing more detailed comparisons between different samples.

5.2. LAM-ICP MS analyses

Trace element analyses of micro-milled clinopyroxene and plagioclase crystals were performed by ***LAM-ICP MS. ……. To be written from Vannucci + Tiepolo……***

5.3. Micro-Sr isotope analyses

Olivine and clinopyroxene were separated at the CNR-IGG in Pisa for Sr isotope microanalyses. After crushing and sieving, samples were 1000-500-250-160 μm grain sizes. Mineral separates were obtained firstly using a Frantz magnetic separator, purified by handpicking under binocular microscope, then cleaned ultrasonically and dried with pure acetone. Some groundmasses were separated by handpicking from the crushed whole-rock samples.

In-situ Sr-isotope microanalyses were performed on glassy groundmasses and on plagioclase and clinopyroxene crystals by microdrilling technique (Fig. 2) using a New Wave™ MicroMill™. Micromilling and extraction of strontium at the nanogram level were carried out following the method proposed by Charlier et al. (2006) at the Department of Earth Sciences, University of Durham (UK). Sample loading and mass spectrometry were executed at the Department of Earth Sciences, University of Florence (IT).

60-150μm polished thick sections were chosen for micromilling. Prior to microsampling, optical investigations and *in-situ* analyses of major and trace elements were carried out by electron microprobe and LAM-ICPMS in order to check the typical and most extreme element zoning. Information on the Sr content at the sample sites allows determining the sample volume needed for each zone to be milled.

Tungsten carbide conical drill bits were used for milling samples from thick sections at depths varying from 50 and 70μm.

The milling was carried out under a single drop of Milli-Q water, in order to cool and lubricate the bit, and to prevent the fine sample dust from being dispersed over the sample surface making recovery more difficult. The efficiency of the recovery (based on comparing calculated sample mass from the excavation geometry to the actual mass of sample) was in the range of 80-85%.

The extraction of strontium at the nanogram level was carried out using micro-columns for standard chemical separation technique (SrSpec™ resin). Blank contamination levels were monitored regularly, although such resulting small contributions preclude the need for any corrections to the sample sizes and the range of $^{87}Sr/^{86}Sr$ analysed in this study. Precisely, considering a micro-sample containing 3ng Sr (typically 3-15ng Sr) and an average blank of ~12pg, contamination levels were <0.5% of the total Sr present.

Sr was loaded on single Re filaments. The Parafilm™ was melted onto the filament surface, leaving a gap to constrain the sample droplet to the centre of the filament. The TaF5 activator (0.7µL)(Charlier et al., 2006) and the sample (taken up in 1µL of 16M HNO_3) were sequentially loaded into the gap. Once the sample was dry, the current was progressively increased to burn off the Parafilm™ and until a dull red glow was achieved for a few seconds. The current on the filament was then turned off and the filament lastly covered by a very thin layer of activator (0.2µL). Afterwards, the filament was ready to be loaded directly onto the magazine of the mass spectrometer.

Sr isotope ratios were measured on the Thermal Ionisation Mass Spectrometer Finnigan Triton TI© (TIMS) equipped with 9 movable collectors. Amplifier gains were calibrated at the start of each day and baselines were measured for before the start of each analysis. ^{87}Sr were aligned in the axial cup and the data collected in 18 blocks of 15 cycles with each cycle having an integration time of 4s. The amplifier rotation option available on the 'virtual amplifier' of the Triton was used during the analysis to eliminate all gain calibration errors. $^{87}Sr/^{86}Sr$ values were measured statically and corrected using an exponential mass fractionation law to $^{86}Sr/^{88}Sr = 0.1194$ respectively, as described in Avanzinelli et al. (2005). Replicate measurements of NBS 987 (0.710249, Thirlwall, 1991) standard (10 ng Sr) during the period of these analyses gave mean values of $^{87}Sr/^{86}Sr = 0.710252\pm0.000011$ (2σ, n =36). Long term mean values measured over the years 2003-2005 for NBS 987 Sr standard were $^{87}Sr/^{86}Sr = 0.710250\pm0.000012$ (2σ, n = 147). Sr isotope measurements were usually performed on beam intensities of 4–6V ^{88}Sr, with ^{85}Rb intensities of <1mV.

6. Compositional characteristics of the 2002-2003 products

Lavas and scoria samples collected during the 2002-2003 eruptive crises have not shown significant variations of texture and bulk chemical and glassy groundmass compositions with respect to those of the HP-magmas erupted during the past decades. Indeed, they bear about 50 vol.% of phenocrysts and microphenocrysts (45-55 vol%), with the most abundant phase being

plagioclase (28-36 vol%), followed by clinopyroxene (10-16 vol%) and olivine (4-7 vol%). They are still shoshonitic basalts with SiO_2 48.5-50.4 wt% and K_2O 2.1-2.4 wt%.

Even the mineral chemistry of the 2002-2003 HP-products do not differ from that of the scoria bombs and lavas erupted from the Strombolian activity in the previous years. Plagioclase is An_{90-60}, clinopyroxene is diopside-augite in composition (Mg#: 0.72-0.92) and olivine Fo_{69-74}. The oscillatory chemical zoning (Fig. 3) and the solid/liquid equilibrium compositions of each mineral phase are similar to those of the previous products. The An content of plagioclase rims is around 65% in the December and January lavas, but decrease up to 60% in the lava flows of March and onwards, due to the decline of the effusion rate after the beginning of the eruption (Landi et al. 2006, 2008 and references therein).

Time variations of whole-rock major and trace element contents during the 2002-2003 effusive events are very small. Only a slight decrease of the most incompatible trace element contents is evident after the 5-April paroxysm (Landi et al. 2006, 2008 and references therein).

The pumices (LP-magma) erupted by the 5 April paroxysm have whole-rock, matrix glass and mineral compositions generally similar to those of their analogues from previous paroxysms. The 2003 pumices, however, do not contain stable high-MgO olivine, usually typical of large-scale paroxysms, and have slightly lower compatible element contents than the previously erupted pumices (Métrich et al., 2005; Francalanci et al., 2008).

6.1. Sr-isotope and trace element microanalytical results

Sr isotope ratios of whole-rocks and groundmasses of lavas slightly decrease with time, passing from 0.706163±5 to 0.706146±7 and from 0.706161±12 to 0.706134±7, respectively (Fig. 4; Table 3a,b). The decrease is more accentuated after the paroxysm, starting from May for the groundmass and June for the whole-rocks. In the samples where Sr isotope data are available on whole-rock and groundmass, it is evident that the groundmasses generally have slightly lower Sr isotopes than the respective whole-rocks, a part from some samples of pre-paroxysm period (the onset lavas and 6 March samples). This behaviour is particularly clear in the samples from the May lavas onwards.

In respect with the previous HP products erupted during about the last decade (up to June 2002), only the onset lavas have similar Sr isotope ratios, whereas the lavas erupted from February onwards show lower $^{87}Sr/^{86}Sr$ values.

The matrix glass of the scoria (HP-magma) erupted by the 5-April paroxysm has Sr isotope ratios similar to those of the groundmass of lavas erupted since two months before and nine days later. The $^{87}Sr/^{86}Sr$ values of pumice samples (LP-magma) erupted by the 5-April paroxysm are

lower than those of the HP-products and similar to those of the LP-products erupted by the previous major explosions during the 1996-2000 period.

For the purposes of mineral microanalysis, the analysed crystals have been generally subdivided in hypothetical zones that, from the internal to the external part, are called "core, outer-core, inner-rim, rim and outer-rim". These zones are commonly defined by compositional zoning or by variable sieved textures of the crystal analysed. The mineral microdrilling for Sr isotope data, however, does not always interested the single zones but, sometimes, it included different crystal zones in a single micro-drilled portion of the mineral. The different cases of microdrilling can be observable in Figure 2 for the 28-December-2002 lava sample, which is reported as example for all the other samples. The milled zones in the plagioclases Pl3 and Pl1 are narrow and well defined, but in the plagioclase Pl2 and Pl4 the intermediate and external drilled portions include different mineral zones (Figs. 2, 5a).

Results of micro-Sr isotope analyses have shown a large isotopic variability (overall between 0.706647±11 – 0.705966±12), even in a single sample, and a persistent isotopic disequilibrium both inside the crystals and between mineral-groundmass. These characteristics are found in all the samples analysed and especially in those from the post-paroxysm lavas. Indeed, in the pre-paroxysm lava samples and in the syn-paroxysm scoria, whole-rock has Sr isotope ratio similar or close to that of the corresponding groundmass, although most of the internal zones of the analysed crystals have $^{87}Sr/^{86}Sr$ values higher than those of the groundmass. The analysed outer-rims, moreover, have $^{87}Sr/^{86}Sr$ values similar to those of the groundmass (Figs. 5a, 6a, 7a). In the post-paroxysm lava samples, all the analysed crystal zones generally have $^{87}Sr/^{86}Sr$ values higher than those of the whole-rocks which, in turn, have Sr isotopes higher than those of the respective groundmasses (Figs. 6b, 8a, 9a).

As for the separated single crystals, their Sr isotope ratios fall in the isotopic range found for the crystal zones and some of them are in equilibrium with the groundmass value. The latter case seems to be particularly found in the olivine crystals which, among three crystals analysed, only the one analysed in the 14-April-2003 lava sample is found in disequilibrium (Figs. 4-9, Tables 3a,b).

In the 28-December-2002 lava sample (the onset lava) (Fig. 5a), a single separated clinopyroxene crystal and the drilled external part, not zoned, of a large clinopyroxene (Cpx13) have given higher $^{87}Sr/^{86}Sr$ values than the groundmass value (Fig. 2, 5a, Tables 1,3a). The analysed plagioclase crystals generally have Sr isotope ratios between 0.70625 and the value of whole-rock and groundmass (0.70616), except for the core of plagioclase-Pl1 showing the high value of 0.70665. Three plagioclase crystals (Pl1, Pl2, Pl4) display the same trend of decreasing $^{87}Sr/^{86}Sr$ from core to outer-rims, whereas in the plagioclase-Pl3 the highest $^{87}Sr/^{86}Sr$ is found in the outer-

core. The external parts of the drilled plagioclase crystals generally have $^{87}Sr/^{86}Sr$ values close to the groundmass values, especially for the outer-rims of plagioclase-Pl1 and -Pl4.

Trace element analyses were performed on crystal zones without sieved textures or fluid inclusions. Thus, they were analysed in inner- and outer-rims of plagioclase-Pl2 and -Pl4 (An% between 64-71) and on the external part of the clinopyroxene-Cpx13 (Mg# = 0.74). Chondrite-normalised (Anders and Grevesse, 1989) patterns for these data are plotted in figures 5b,c,d. In respect with chondrite values, plagioclases are mostly enriched in Ba, Sr, Eu and LREE (light rare earth elements). REE are negatively fractionated and positive Eu anomalies are not correlated with the An content (Figs. 5b,c; Table 2a). Clinopyroxene patterns are particularly enriched (>10 chondrite) in Hf, Zr, Sc and REE, which show a bell shaped pattern for LREE and negative Eu anomalies (0.7-0.8) (Figs. 5d; Table 1).

In the 06-March-2003 lava sample, two plagioclase crystals drilled for Sr isotope analyses (Pl2, Pl3) show a decrease of $^{87}Sr/^{86}Sr$ from core to rim, whereas plagioclase-Pl4 has the opposite trend. $^{87}Sr/^{86}Sr$ values are generally lower than 0.70630, with rims of plagioclase-Pl2 and -Pl3 having values close to the groundmass values (Fig. 6a; Table 3a).

In the 5-April-2003 scoria and pumice samples, Sr isotope ratios of the analysed minerals are lower than 0.70630, except for a higher ratio (0.70640) found in the plagioclase-Pl3 core. The internal part of the clinopyroxene-Cpx1, including a large diopsidic outer-core (Mg# = 0.89), has a $^{87}Sr/^{86}Sr$ value (0.70597) significantly lower than the groundmass values, whereas its outer-rim is in equilibrium with the groundmass. Similar $^{87}Sr/^{86}Sr$ values to those of the groundmass are also found in a separated olivine crystal and in the plagioclase-Pl1 core (Fig. 7a; Table 3a), which shows the highest $^{87}Sr/^{86}Sr$ in its outer-core. Plagioclase-Pl2hP, found in the pumice, displays an increase of $^{87}Sr/^{86}Sr$ from outer-core to rim.

Chondrite-normalised trace element patterns of plagioclase are similar to those reported for plagioclase of the 28-December-2002 sample (Figs. 7b,c,d,e). Trace element patterns of rim and inner-rim of Cpx1 are similar to the patterns of Cpx13 analysed in the onset lava flow, but the outer-core of Cpx1 shows a pattern shifted towards lower trace element contents (Figs. 5d,e). The latter characteristic of Cpx1 outer-core is correlated with its higher Mg# and lower $^{87}Sr/^{86}Sr$ value. The pattern of Cpx1 outer-core also has no Eu anomaly and less fractionated LREE in respect with the patterns of the other Cpx1 zones (Fig. 5e; Table 1).

In the 13-May-2003 lava sample a separated clinopyroxene has $^{87}Sr/^{86}Sr$ value nearly similar to the groundmass value. The two drilled plagioclase crystals, including their outer-rims, show Sr isotope ratios between 0.70630 and 0.70620, which is higher than the groundmass value (0.70614) (Fig. 6b).

In the 17-May-2003 lava sample, a separated single olivine and a single clinopyroxene crystal have $^{87}Sr/^{86}Sr$ values analogous or higher (0.70623) than the groundmass value (0.70614), respectively. The drilled zones of three plagioclase crystals (Pl1, Pl2, Pl3) and of one clinopyroxene (Cpx2) have shown $^{87}Sr/^{86}Sr$ values between 0.70618 and 0.70624, also including some outer-rims and consequently indicating isotopic disequilibrium with the residual liquid (Fig. 8a).

Chondrite normalised trace element patterns for plagioclase and clinopyroxene are similar, in shape and contents, to the patterns of the same minerals in the previous samples (Figs. 5b-e, 7b-e, 8b-e). No correlation seems to be present in plagioclase between An contents and trace element characteristics, whereas in the clinopyroxene-Cpx2, the higher Mg# of outer-core is correlated with the lower trace element contents and the lack of Eu anomaly (Fig. 8e), as it occurs in Cpx1 of 5-April-2003 scoria sample (Fig. 5e).

In the 20-July-2003 lava sample (the last erupted lava), a separated clinopyroxene crystal has Sr isotope ratio of 0.70618, which is not in isotopic equilibrium with the groundmass, having a lower ratio (0.70613) (Fig. 9a). This is also the condition of plagioclase-Pl2 and -Pl3, especially the Pl2 crystal with $^{87}Sr/^{86}Sr$ between 0.70638-0.70631. Only the external part of Pl1 has a lower $^{87}Sr/^{86}Sr$ value (0.70615), close to the groundmass value (Fig. 9a, Table 3b).

Chondrite-normalised trace element patterns of plagioclase show similar characteristics to the previously described plagioclases, with no correlations between trace elements and An content or Sr isotope ratios (Fig. 9b,c).

7. Discussion

The microanalyses reported in this paper on the products erupted during the 2002-2003 eruptive crisis show a more complex magmatic system than that previously figured out on the bases of the whole-rock data (e.g., Metrich et al., 2005; Landi et al., 2006, 2008; Francalanci et al., 2008). In respect with the other geochemical and mineralogical data, Sr isotope ratios on whole-rocks more significantly change along the course of the effusive event. They only show, however, a tiny decrease after February 2003 which becomes slightly more accentuated in the June- and July-2003 samples (in general from 0.706165 to 0.706145) (Fig. 4). Instead, the micro-Sr isotope ratios reported here point out variable isotopic disequilibria between the different zones of plagioclase and clinopyroxene and between minerals and groundmass, with a larger variation of $^{87}Sr/^{86}Sr$ values, ranging from 0.70597 to 0.70665 (Figs. 5-9).

Comparing the Sr-isotope data of whole-rock/groundmass pairs of the samples analysed from the 2002-2003 products, it is evident that some samples of lavas erupted before 5-April-2003 paroxysm

have similar values in whole-rock and groundmass, whereas in most of the other samples, and especially in those from May-2003 onwards, the groundmass has systematically lower Sr isotope ratios. On the other hand, all the analysed samples contain phenocrysts in isotopic disequilibrium with the groundmass, having generally higher Sr isotope values (up to 0.70665; Fig. 5a), but also lower $^{87}Sr/^{86}Sr$ as the case of the Cpx1 core of 5-April-2003 scoria (0. 0.70597; Fig. 7a). Obviously, only the separated minerals and crystal outer-rims having $^{87}Sr/^{86}Sr$ value similar to that of the respective groundmass are in equilibrium with the host liquid.

These data will be discussed and interpreted in the lights of the present knowledge on the dynamics and plumbing system configuration at Stromboli, which will be briefly resumed in the following section.

7.1. State of the art on the dynamics and plumbing system of the present-day activity

Since its beginning, the Strombolian activity has been dominated by the interplay between magmas having contrasting density and viscosity: the shallow, crystal-rich and degassed magma (HP-magma) and the nearly-aphyric, volatile-rich magma of deeper derivation (LP-magma). These magmas are sited in a polybaric multi-reservoir plumbing system and interact in different ways (mingling - mixing), depending on the variable eruptive dynamics (Francalanci et al., 1999, 2004, 2005).

The LP-magmas are sited at a lithostatic pressure of 190-250 MPa, as derived from the H_2O-CO_2 dissolved contents (initial water content of about 3.0 wt%) of melt inclusions in equilibrium olivine. They derive from their volatile-rich parental melts by crystal fractionation of mafic phases. These calculated pressures give a magma pond zone located at ~7-10 km depth (Métrich et al., 2001, 2005, 2010; Bertagnini et al., 2003). The LP-magma reservoir is periodically recharged by a mafic Ca-rich magma with relatively low Sr isotope ratios (~0.70608) and containing CO_2-rich gas phase (Francalanci et al., 2005; Métrich et al., 2010).

The quite similar basaltic composition of the erupted HP-/LP-magmas (scoria/pumice) pairs, which contrasts with the marked difference in their crystal and volatile contents, has been interpreted as an example of crystallization driven by water-loss at very low pressure level which moves the LP-magma composition to that of the HP-magmas (Métrich et al., 2001; Bertagnini et al., 2003). Nevertheless, the different Sr isotope characteristics of the HP- and LP-magmas suggested a much more complex plumbing system, in which the HP-magmas reside at a shallow level of ~2-3 km depth. This magma rest zone was firstly hypothesized in order to explain the homogeneous Sr isotope data of the HP-magmas (Francalanci et al., 1999, 2004), taking also into account the possible remnant of an old structure at this pressure level (Vaggelli et al., 2003). A magma storage

zone at ~1-3 km depth has been later suggested also on the basis of gas plume composition calculations (Aiuppa et al., 2009; Allard, 2010) and of melt inclusion data (Métrich et al., 2010).

The dissolved water content of LP-magma is high enough to prevent plagioclase crystallization, except at the ultimate stages of its transfer to the surface when the water loss at lower pressure, drives the melt composition towards the stability field of plagioclase. On the contrary, plagioclase is the dominant mineral phase of the shallow degassed HP-magmas where it crystallizes in equilibrium with clinopyroxene and olivine (e.g., Francalanci et al., 2004; Landi et al., 2004; Di Carlo et al., 2006; Bertagnini et al., 2008).

Minerals in scoria record strong chemical, isotopic and textural heterogeneity providing evidence of repeated and discrete arrivals of water-rich, less Sr radiogenic LP-magmas in the shallow system. The HP-magmas, therefore, undergo crystallization of olivine, pyroxene and plagioclase together with periodic mixing with the refreshing volatile-rich LP-magmas which determines crystal dissolution. The mixing process, favored by vigorous convection, leads to maintain the uniform compositional characteristics of the HP-magmas with time and, in particular, to re-homogenize the Sr isotopes. An efficient mixing is possible because the HP-magmas in the shallow reservoir are not fully degassed when they interact with the LP-magmas, thus the two magmas have more similar rheological characteristics. Further degassing and crystallisation occur as the HP-magmas move through the conduits to the surface, thus reaching their high crystal content. The overall decrease of Sr isotope ratios with time in the HP-magmas starting from 1980-1985 was due to the nearly coeval decrease of $^{87}Sr/^{86}Sr$ values in the replenishing LP-magmas. The LP-magmas erupted by the different-scale paroxysms are usually deeply mingled with the coeval HP-magmas (syn-eruptive scoria-pumice mingling) because only in those cases they arrive directly to the surface without mixing with the HP-magmas at shallow levels (Francalanci et al., 1999, 2004, 2005; Armienti et al., 2007; Fornaciai et al., 2009).

In addition to the previously mentioned magma rest zones, the presence of an intermediate cumulus crystal-mush body, where plagioclase and pyroxene recorded the highly variable and high Sr-isotope signature of the previous magmas, was also proposed for explaining the large Sr isotope disequilibrium found in plagioclase and clinopyroxene of products erupted in 1984, 1985 and 1996. During the periodic magma recharge events, LP-magma passes through the cumulus reservoir sampling minerals and transporting them into the shallower reservoir. These minerals can be resorbed before a crystal zone in equilibrium with LP-magmas forms around them due to degassing at shallow level (Francalanci et al., 2005).

Finally, a topic of recent discussion is the respective role of magma and/or gas in triggering the paroxysmal eruptions. The rapid ascent, from a depth of 7-10 km, of bubbly LP-magma blobs in

which magma remains in equilibrium with its gas (Métrich et al., 2010) is opposite to the hypothesis of the catastrophic ascent of CO_2-rich gas blobs formed by intermittent collapse of bubble foams accumulated at sill-like discontinuities below the volcano (from 3 up to 10 km deep depending on the paroxysm energy) (Allard, 2010).

7.2. Significance and age of the high Sr-isotope crystal zones

Cores of plagioclase and clinopyroxene crystals, usually resorbed, with higher Sr-isotope ratios than those of the groundmass values (up to 0.70635) were already found in samples of the present-day activity of Stromboli, specifically in the 1984, 1985 and 1996 scoria, lava and pumice. They have a variable chemical composition (An_{58-85} and Mg# 0.70-0.90, respectively) and were considered to derive from a cumulus crystal mush reservoir formed during the previous activity (Francalanci et al., 2005). Hence, these crystals are grown in and recycled from closely related progenitor magmas and they can be called "antecrysts" according to Davidson et al. (2007).

The results reported in the present paper indicate that these antecrysts, generally found as inner and resorbed parts of the most zoned phenocrysts, are still present on the 2002-2003 Stromboli magmas (Figs. 2, 5-9). Furthermore, bulk minerals with higher Sr-radiogenic than their host groundmass, separated from samples of the following 2007 lava flows, still point to the presence of antecrysts in these magmas (Landi et al., 2009). The occurrence of recycled minerals inherited from the previous activity, therefore, is not a phenomenon of a specific period of activity, but it is a characteristic of the present-day plumbing system of Stromboli and, together with the HP- and LP-magmas, it represents a significant component contributing to the persistence of the typical steady state conditions of this volcanic system.

According to petrographic observations and considering the most zoned minerals, the amount of antecrysts may be roughly estimated at 1/3 of the total crystal content (around 17 vol%).

On the bases of $^{87}Sr/^{86}Sr$ values of the high Sr-isotope antecrysts, it is possible to hypothesise the period of activity during which they crystallised. Indeed, the subaerial rocks of Stromboli have variable Sr isotope ratios (Fig. 1) with the highest values, ranging between 0.70660-0.70760, found in the potassic rocks of the Neostromboli period (13-6 ka). Starting from the end of this period and for all the following Recent period, the $^{87}Sr/^{86}Sr$ values of the erupted products generally decreased with time until the present-days, starting from 0.70669 ("Pizzo-Sopra-la-Fossa tuff") to 0.70615 (current volcanic activity). The antecrysts of the 2002-2003 rocks have a Sr-isotope range between 0.70665 - 0.70617, which perfectly encompasses all the values of the Recent period products. The highest antecryst value of 0.70665, however, could also record the Neostromboli activity, thus possibly indicating also recycling in the present-day system of older crystals formed during the

Neostromboli period (13-6 ka). Nevertheless, Neostromboli rocks are potassic trachybasalts with higher trace element and potassium contents than the shoshonitic basalts of the Recent period. Accordingly, comparing the trace element composition of minerals, it is possible to exclude the Neostromboli period for the provenience of these antecrysts (Fig. 10). Indeed, K_2O of plagioclase and trace element contents of clinopyroxene of the 2002-2003 products, never overlain the compositional field of the potassic rock minerals (i.e., KS series of Neostromboli period), but they show the typical mineral compositions of the Stromboli shoshonitic series (Fig. 10). Thus, the latter characteristic, together with the high Sr-isotope value (the pre-Neostromboli shoshonitic activity has Sr-isotope ratios lower than 0.70620, Fig. 1), constrain the provenience of the high Sr-isotope antecrysts from the Recent period.

The Recent period of activity includes several volcanic events, occurring after the potassic Neostromboli period until the present-days, and mainly emplacing the "Pizzo-Sopra-la-Fossa tuff cone", "San-Bartolo lavas", "Post-Pizzo series", "sub-Recent-Sciara lavas" and the "Sciara products" (Hornig-Kjarsgaard et al., 1993; Petrone et al., 2004, 2006). Specifically, the shoshonitic basalts of "Pizzo-Sopra-la-Fossa tuff cone", with the highest Sr-isotope ratios of the Recent period (up to 0.70669) (Petrone et al., 2004; Di Salvo, 2010), are also the oldest products of this period, having an age of about 2.5 ka (Rosi et al., 2000; Speranza et al., 2008; Di Salvo, 2010). This limits the crystallization age of the antecrysts with the highest Sr-isotope ratios at a period not older than about 2.5 ka.

Furthermore, it is important to note that most of the $^{87}Sr/^{86}Sr$ values (ca. 80%) measured in the high Sr-isotope antecrysts (crystals with $^{87}Sr/^{86}Sr$ > ca. 0.70618) of 2002-2003 products, is lower than 0.70628, which is the highest value registered in the present-day activity during the twentieth century and possibly during the last 600 years (Francalanci et al., 1999, 2004 and unpublished; Speranza et al., 2008). This means that these crystals could be possibly crystallised in the last hundreds years and recycled by the dynamics of the present-day Strombolian activity.

7.3. Significance of the low Sr-isotope crystal zones

A crystal zone with chemical (high An% or Mg#) and Sr-isotopic (low $^{87}Sr/^{86}Sr$) composition in equilibrium with the LP-magmas, was found around the high-Sr-radiogenic cores of 1984 and 1996 scoria, leading to hypothesise these cores were brought into the shallow HP-system by the refreshing LP-magma, which passes through the crystal mush reservoir, "collects" the crystals and leads to crystallise a low Sr-isotope crystal zone around the cores (Francalanci et al., 2005). In the micro-Sr isotope data of 2002-2003 lavas, crystal zones with low Sr-isotope ratios (in equilibrium with LP-magmas) around the high Sr-radiogenic cores are not found. A possible reason is that these

crystal zones are not drilled because they are quite thin. An example of this could be the clinopyroxene-Cpx2 of figures 8a,e, in which between the drilled core and outer-rim there is an un-drilled, light and thin, intermediate zone with MgO-richer composition and lower REE contents than its core and rim (see also Fig. 11 and the sketch of this crystal in Fig.12). Furthermore, the same situation also occurred in the 1985 lava sample of Francalanci et al. (2005) and it was ascribed to the large size of the drilled crystal zones. A similar reason could be also attributed to the lack of these low Sr-radiogenic crystal zones in the 2002-2003 samples. Indeed, an example is shown in the plagioclase-Pl2 of figure 2 in which the external drilled zone includes the inner-rim An_{71}, the rim An_{80} and the outer-rim An_{69}. The thin and sieved rim with high An content (An_{80}) could be probably crystallised in the LP-magmas during its degassing at shallower level before mixing with the HP-magma (e.g., Francalanci et al., 2004, 2005; Landi et al., 2004); thus, it might be a possible zone having low $^{87}Sr/^{86}Sr$, but it is drilled together with the larger inner-rim and outer-rim having lower An contents.

It is probable that most of the inner crystal zones with lower Sr-isotopes than the respective external zones (e.g., Pl3 of 28-December-2002, Pl4 of 6-March-2003, Pl1 of 5-April-2003 scoria; Figs. 5-7), also includes low Sr-isotope crystal zones, crystallised by LP-magmas throughout the entire history of the mineral. Indeed, due to the general Sr-isotope decrease with time during the Recent period of Stromboli activity starting from Pizzo-Sopra-la-Fossa, a similar trend should be registered from cores to outer-rims of the mineral phases. This expected trend is effectively the most common among the analysed crystals (Figs. 5-9, 11).

Only one lower $^{87}Sr/^{86}Sr$ value than the groundmass value, is resulted in the internal part of the clinopyroxene-Cpx1 from 5-April-2003 scoria (0.70597) (Tab. 3a; Figs. 7a, 12). This part also includes a large diopsidic outer-core with Mg# 0.89 that could be crystallised from an LP-magma, as also corroborated by its lower incompatible trace element contents (Fig. 7e). Because the lowest known $^{87}Sr/^{86}Sr$ value of LP-magmas is 0.70605 in 1996 products (Francalanci et al., 2005; 2008), the low $^{87}Sr/^{86}Sr$ value of Cpx-1 outer-core can testify that the Sr-isotope ratios of previous LP-magmas were even lower than 0.70605.

The presence of low Sr-isotope crystal zones is also proved by calculation for balancing the Sr-isotope ratios in the analysed samples. In particular, it is significant to consider the case where the whole-rock value is similar to the groundmass value as it happens, for example, in the sample of 28-December-2002 (Fig. 5a). Because the high Sr-isotope antecrysts are also present in these samples, a certain amount of low Sr-isotope crystal zones needs in order to balance the average Sr-isotope ratio of crystals with that of the groundmass (or the whole-rock). If the average Sr content of crystal zones is considered similar for the two types of crystals in disequilibrium with the groundmass (i.e.,

high and low Sr-isotope crystal zones), the relative amount of low Sr-isotope crystal zones will depend on the $^{87}Sr/^{86}Sr$ values assumed for the two end-members. For the high Sr-isotope end-member it is reasonable to use the average $^{87}Sr/^{86}Sr$ value calculated among all the high Sr-isotope antecrysts of 2002-2003 products (i.e., the average of 37 data higher than 0.70618 is 0.70624, which is nearly similar to the averages calculated in the single samples). For the low Sr isotope end-member the lowest value measured (0.70597) or the value of LP magma erupted by the 5-April-2003 paroxysm (~0.70610) can be considered. Accordingly, 30/70 and 50/50 proportions (wt%) between low/high Sr-isotope crystal zones are calculated, respectively. Considering that only one low Sr-isotope crystal zone has been drilled, the former proportions seem to be more reasonable, possibly suggesting the presence of low Sr-isotope crystal zones with lower $^{87}Sr/^{86}Sr$ values than that of 5-April-2003 LP-magma. Based on the petrographic estimation of about 17% of antecrysts (the most zoned crystals: about 1/3 of total crystal content), we may roughly calculate 12% of high Sr-isotope antecrysts (17x0.7) and 5% of low Sr-isotope crystal zones on the total rock.

7.4. Variations along the effusive event: interaction between LP- and HP-magmas

The whole-rock and mineral chemistry data on the products erupted during the 2002-2003 crisis have shown that the shallow magmatic system is still maintained in the steady-state conditions which characterised the system in the last decades. The general uniform bulk composition of the erupted lava indicates the presence of a considerable volume of homogeneous HP-magma residing in the shallow plumbing system of the volcano (assuming a lava vesicularity of about 30 vol.%, about 0.0088 km^3) (Landi et al., 2006, 2008; Marsella et al., 2008).

The slight but systematic variation of the most incompatible trace elements and of the Sr-isotope ratios between bulk-rocks erupted before and after the 5 April paroxysm are suggested to be generated by limited mixing (about 20%) between the fresh, volatile-rich LP-magma, erupted as pumice during the paroxysm, and the volatile-poor HP-magma feeding the lava flow (Landi et al., 2006, 2008). In the lights of the micro-analytical data reported here, although the decrease of Sr isotope ratios during the lava effusion could be also determined by a decreasing amount of high-Sr antecrysts, the corresponding decrease of $^{87}Sr/^{86}Sr$ values in the groundmasses from the onset to the end lavas (Fig.4) is a clear signal of the mixing with low Sr-isotope LP-magmas similar to those erupted by the 5-April paroxysm. It can be calculated at about 30% the amount of LP-magma mixed with HP-magma for decreasing the $^{87}Sr/^{86}Sr$ values of the groundmass from the beginning (0.706161) to the end (0.706134) of the lava effusion. If a similar calculation is performed using the whole-rocks (from 0.706160 to 0.706146), however, this amount is reduced to about 22%. This discrepancy of about 8% can be explained by an increased content of high Sr-isotope antecrysts

towards the end lavas. It is worthy noting that a similar amount of high Sr-isotope antecrysts (with average Sr-isotope ratio of 0.70624) is necessary in the 20-July lava sample for explaining the difference in Sr-isotope ratios between the whole-rock (0.706146) and the groundmass (0.706134). This increased amount of high Sr-isotope antecrysts towards the end lavas, associated with the decrease of Sr isotope ratios in the groundmasses, could be brought in the shallow system by the increased arrival of LP-magmas which pass through the crystal mush zone and carry the previously formed crystals, in agreement with the already proposed hypothesis (Francalanci et al., 2005). This is further corroborated by the presence in the post-paroxysm lavas of high Sr-isotope antecrysts with outer-rims in isotopic disequilibrium with the groundmass (Fig. 11), suggesting a very short residence time for these antecrysts in the shallow system.

The above mixing calculations have been performed between the beginning and the end lavas. Nevertheless, although the slight decrease of trace element contents seems to commence after the 5-April paroxysm, the Sr isotope ratios of the groundmasses begin to slightly but significantly decrease from February, for decreasing at higher extent from May to July. Furthermore, the $^{87}Sr/^{86}Sr$ values of groundmasses in the scoria erupted by the 5-April paroxysm and in the following 14-April lavas, are similar. This suggests that: i) the arrival of LP-magmas at shallow levels and their mixing with HP-magmas seem to be also occurred before the 5-April paroxysm; ii) the rapid ascent of LP-magmas to the surface during the paroxysm does not immediately affect the composition of the shallow HP-magmas, although the two magmas use the same conduit to the surface (Pistolesi et al., 2008 and reference therein), but it possibly affects the composition of lavas erupted one month after the paroxysm. The evidence at point (i) is also corroborated by the occurrence of few LP glassy shards in ashes erupted on 8-March-2003 (Schiavi et al., 2010), together with changes in fluid geochemistry (Aiuppa and Federico 2004; Carapezza, 2004) and lowering of Sr isotope ratios in scoria groundmasses (Landi et al., 2008) during October-November 2002. As for the considerations at point (ii), it is also worthy noting that the mineral bulk compositions and zoning patterns of post-paroxysm lavas do not change, maintaining the typical crystal outer-rim compositions in equilibrium with the HP-magmas (Francalanci et al., 2004; Landi et al., 2006, 2008); furthermore, no variations in the crystal size distribution of lavas are found immediately after the paroxysm, and the decrease in nucleation density observed in the 20-July lavas can be considered to be the only petrographic effect of the arrival of LP magmas in the shallow system (Fornaciai et al., 2009).

Thus, different data do not seem to suggest the same processes: Sr-isotopes of groundmasses pointed out that HP-magmas mixed with an increased amount of LP-magmas from the beginning to the end of the effusive event, up to a maximum of 30% of LP-magmas in the 20-July lavas,

although the mixing seems to be not directly related to the 5-April paroxysm; petrographic and mineralogical characteristics, however, do not show the occurrence of this mixing process. We previously hypothesized, however, that efficient mixing between HP- and LP-magmas takes place in a shallow reservoir sited about 2-3 km depth, where the two magmas have more similar rheological characteristics, and a further crystallisation driven by degassing occurs during the residing of magma inside the open conduits to the surface (Francalanci et al., 2005). The existence of the HP-magma reservoir at intermediate level was later proposed by other authors on the bases of different data (e.g., Aiuppa et al., 2009; Allard, 2010; Métrich et al., 2010), although other authors still propose a continuous conduit from the deep LP-magma reservoir to the surface (Burton et al., 2007; Schiavi et al., 2010). It can be, therefore, hypothesized that the LP- and HP-magma mixing evidenced by Sr isotope ratios of 2002-2003 lava groundmasses, occurred in this shallow reservoir. The following crystallisation in the conduit lead to re-equilibrate the mineral composition and the petrographic textures to those typical of HP-magmas and to generate at least 0.0088 km^3 of HP-magma erupted as lava flows. The presence of crystal outer-rims in Sr-isotopic equilibrium with the groundmass in the pre- and syn-paroxysm products indicates that crystallisation occurred after mixing (Figs. 5-9, 11). Considering the maximum growth rate calculated for these plagioclase crystals (10^{-9}-10^{-8} cm/s; Armienti et al., 2008; Fornaciai et al., 2009), a 0.1 mm large outer-rim forms in a time range between several days to some months. This suggests that a considerable amount of LP-magma arrived in the shallow reservoir before the onset of the lava flows.

Schiavi et al. (2010) find different compositions for the LP-magmas erupted as glassy shards in ash fallouts on 8-March-2003 in respect with those erupted on 10-April-2003, which have typical LP-magma compositions. In particular, the former show higher contents of both incompatible trace elements (including Sr) and Ni, Cr, V. The authors explain this anomalous LP-magma composition by fractional crystallization of clinopyroxene and olivine associated with minor assimilation of dunite and wehrlite assemblages during a slower ascent rate to the surface of a small volume of LP-magmas occurred on 8-March-2003. Alternatively, in the light of our results, the pre-paroxysm LP-ash shards could represent the ascent to the surface of LP-magma already present in the shallow reservoir during its mixing with the HP-magma (leading to the increase of incompatible trace element contents) associated with resorption of previously crystallised minerals (leading to the increase of Cr, Ni, V and Sr contents). In the authors' hypothesis, small volume of LP-magmas would have continued to rise up from their deep reservoir during the effusive event, directly arriving to the surface. In our alternative hypothesis, the pre-paroxysm LP-magmas would represent those arrived in the shallow reservoir some months before and small batches ascended to the surface probably due to the decrease of the magmastatic pressure during the lava outpouring.

A new input of typical LP-magma from the deep reservoir triggered the 5-April paroxysm by its direct arrival to the surface, passing through the conduit without mix with the HP-magma because of the different rheology of the two magmas. The new LP-magma left in the shallow reservoir, however, started to mix with the interstitial liquid of the HP-magma, leading to the further decrease of Sr-isotopes in the groundmasses of lavas erupted from May onwards. Furthermore, the new LP-magma input also brought more antecrysts in the final lava system and the continuous lava outpouring to the surface inhibited the growth of outer-rims in isotopic equilibrium. This apparently disagrees with the presence in post-paroxysm lavas of bulk olivine and clinopyroxene with Sr-isotopes similar to those of the host groundmass. Nevertheless, the growth rate of olivine and clinopyroxene is respectively twice and fourth times higher than the plagioclase growth rate (Armienti et al., 2007) and the higher undercooling during the lava outpouring should have favoured the nucleation instead of the antecryst rim growth.

7.5. Dynamics of the crystal recycling

Present data on the 2002-2003 eruptive products have shown the presence of high Sr-isotope antecrysts, increasing towards the end lavas (about 12% to 12+8=20%) and recording a period of activity (the Recent period) ranging from about 2.5 years ago to the present time. They are associated with low Sr-isotope crystal zones, crystallized from LP-magmas, possibly in proportions of about 3/7 in respect with the high Sr-isotope antecrysts. These results, together with the continuous decrease of Sr-isotopes with time in the products of the Recent period, seem to indicate a more direct connection between the feeding system of the present-day activity and the source of high Sr-isotope antecrysts in respect with the hypothesis previously proposed. The latter considered the presence of a cumulus crystal mush zone sited generically below the HP-magma reservoir and within the pressure conditions in which plagioclase still crystallises (Francalanci et al., 2005).

Alternatively, we could now suggest that the "Pizzo-Sopra-la-Fossa" magma reservoir was the beginning magma body of the HP-system. Its continuous refilling by lower Sr-radiogenic LP-magmas followed by crystallization, lead to the general trend of decreasing $^{87}Sr/^{86}Sr$ in the Recent rocks and to the formation of the present-day HP-magmas with some antecrysts recording this entire magma history during their growth. This means that the plagioclase cores with the highest $^{87}Sr/^{86}Sr$ values, as for example that with value akin to that of the "Pizzo-Sopra-la-Fossa" magmas (0.70665), are remained in the HP-magma system for about 2.5 ka. Nevertheless, this disagrees with the calculated resident times for this system, which are consistently lower, ranging between 1-30 years (Gauthier and Condomines, 1999; Francalanci et al., 1999). This discrepancy, therefore, suggests again that the old antecrysts are periodically brought into the HP-magma system by the refilling LP-

magmas which pass through a cumulus crystal mush formed since the "Pizzo-Sopra-la-Fossa" activity (Fig. 12). This also agrees with the increase of antecryst content after the 5 April paroxysm. We can now propose, however, that the cumulus zone is part of the HP-magma shallow reservoir and it forms its lower part, being partially re-mobilized by the gas/volatiles-rich LP-magmas, which periodically rise up to refill the HP-magma reservoir (Fig. 12). Due to this process, the latter magma body possibly migrated up with time. Before mixing with HP-magmas, the high Sr-isotope antecrysts can firstly be resorbed by the host LP-magma and then, following degassing at low pressure, a crystal zones in equilibrium with LP-magma can crystallise around the resorbed antecrysts (Francalanci et al., 2005).

Furthermore, these results have also pointed out that about 80% (on 37 measured Sr isotope ratios > ca. 0.70618) of high Sr-isotope antecrysts in the 2002-2003 products can be crystallised in the last hundreds years. This suggests they are recycled by the dynamic processes of the Strombolian activity, which appear to be particularly efficient in recycling crystals considering the high percentage content of these high Sr-isotope antecrysts. On the other hand, whatever the conceptual model of the volcano is proposed, it is nowadays believed that the periodic mild Strombolian explosions leave in the conduit a degassed dense HP-magma descending downwards possibly along the conduit walls (Chouet et al., 2003; Colò et al., 2010; Lautze and Houghton, 2007; Burton et al., 2007; Fornaciai et al., 2009; Metrich et al., 2010). This mechanism leads minerals (with possibly degassed silicate melt) to be also recycled from the upper part of the plumbing system into the HP-magma reservoir. These minerals sink in a hotter, gas/volatile-richer melt (blue down arrows of Fig. 12) undergoing to resorption at different extent depending on the conditions of the host melt (i.e., degree of mixing with LP-magmas, of crystallization and degassing) and possibly on their place in the reservoir. Obviously, no low Sr-isotope crystal zone (i.e., in equilibrium with the LP-magma end-member) can grow on these crystals, except when they are settled in the lower part of the magma body and re-mobilized again by LP-magma inputs (e.g., Cpx2 of Figs. 8, 12).

Thus, this intricate dynamics of crystal recycling, in which minerals (and possibly melts) re-enter in the convective portion of the HP-magma chamber from both lower and upper parts, leads to the complex and multiple zoning of many minerals of the products from the present-day activity (Fig. 12).

8. Conclusions

Several new contributions to the understanding of the present-day system of Stromboli arise from these large number of chemical and Sr-isotope micro-analytical data on the products of the 2002-2003 eruptive crisis.

First of all, we found that the presence of recycled minerals inherited from the previous activity (antecrysts) seems to be a constant characteristic of the present-day plumbing system (Figs. 5-9) which, together with the interaction between HP- and LP-magmas, allows maintaining the typical steady state conditions of this volcanic system.

The $^{87}Sr/^{86}Sr$ values of the high Sr-isotope antecrysts (0.70665-0.70618), associated to their trace element composition, limit the age of these antecrysts at a period (Recent period of activity) not older than about 2.5 ka, starting from the emplacement of "Pizzo Sopra la Fossa" tuff cone to the present-day activity (Figs. 5-11).

As for the dynamics of crystal re-cycling, we propose that antecrysts (and possibly melts) re-enter in the HP-magma reservoir from both its lower and upper parts. From the bottom, they are re-mobilised by ascending LP-magmas from a cumulus crystal much reservoir possibly directly interconnected with the HP-magma reservoir; whereas at the top, the degassed and dense HP-magma left in the conduit by the periodic mild Strombolian explosions, sinks in the hotter and gas/volatile-richer melts residing in the reservoir (Fig. 12).

The presence of low Sr-isotope crystal zones, grown in equilibrium with LP-magmas, is inferred by several considerations and calculations, in a proportion 30/70 (wt%) between low/high Sr-isotope crystal zones. Only one low Sr-isotope crystal zone is drilled in the internal part of a clinopyroxene (Tab. 3a; Figs. 7a, 12), testifying that the Sr-isotope ratios of previous LP-magmas could have been significantly low (0.70597). Based on petrographic estimations, we roughly evaluate amounts of 12% of high Sr-isotope antecrysts and 5% of low Sr-isotope crystal zones on the whole-rock of the onset lava. The high Sr-isotope antecrysts, however, increases their abundance towards the end lavas (up to about 20%), possibly because they are brought by LP-magmas refilling the shallow HP-magma reservoir during 5-April paroxysm.

A sketch of the present-day plumbing system of Stromboli at intermediate pressure (about 2-3 km depth) is reported in figure 12. This is based on the previously proposed hypothesis (Francalanci et al., 1999, 2004, 2005) that efficient mixing between HP- and LP-magmas can only occur in a shallow reservoir where the two magmas have more similar rheological characteristics than in the conduit (i.e., HP-magmas is less degassed and have a lower crystal content than the HP-magma at the surface). Further crystallisation driven by degassing, indeed, is considered to occur in the

conduit during the ascent of magma to the surface. The gas/volatiles-rich LP-magmas firstly promote resorption of the transported antecrysts and then, following degassing at lower pressure and before mixing with HP-magmas, a crystal zones in equilibrium with LP-magma (low Sr-isotope crystal zone) can grow around the resorbed antecrysts (see also Francalanci et al., 2005). Even the antecrysts re-cycled from the top and descending from the degassed conduit can suffer resorption at different extent depending on the conditions of the melt in the HP-magma reservoir (Fig. 12).

As for the dynamics of magma processes during the 2002-2003 eruptive period, the decrease of $^{87}Sr/^{86}Sr$ values in the lava groundmass soon after the onset of the lava flows and the presence of minerals and crystal outer-rims in Sr-isotopic equilibrium with the hybrid groundmass (Figs. 4-7, 11) suggest that a considerable amount of LP-magma (higher than during the normal Strombolian activity) arrived in the shallow HP-magma reservoir before the onset of the lava flows and mixed with the interstitial melt of the HP-magma (Fig. 12). Indeed, a time spans of months was needed to crystallise minerals in isotopic equilibrium with the hybrid melts. This higher amount of LP-magma input can be the cause triggering the lava flow eruption. During the 5-April paroxysm, LP-magma from the deep reservoir directly arrived to the surface, only mingling with the HP-magma in the conduit due to the different rheology of the two magmas. New LP-magma, however, was left in the shallow reservoir, affecting the groundmass Sr-isotopes of lavas erupted about one month later (from May onwards) (Figs. 4, 6, 8, 9, 11) and carrying more antecrysts in the final lava system. The following crystallization in the conduit led the mineral compositions and the rock textures to reach those typical of HP-products (Figs. 2, 12).

Finally, we attempt some considerations on the involved magma volumes and, firstly, we can try an estimation of the conduit volume based on the crystallization time of mafic phases in isotopic equilibrium with the mixed groundmass of 13- and 17-May-2003 (Figs. 6, 8, 11; Table 3b). Based on the hypotheses that mixing occurs in the shallow reservoir and that the effect of mixing with LP-magma of 5-April paroxysm is evident in the lava groundmass of May, these phases would have taken 30-40 days for crystallising from the mixed groundmass during their ascent in the conduit to the surface. It is worthy noting that this time period also corresponds to the growth rate of $3x10^{-8}$ cm/s (the maximum growth rate according to Armienti et al., 2007) for a mafic phase of that size (about 1 mm). Considering an average mass eruption rate of 0.7 m^3/s (= total lava volume divided for the entire period of lava effusion; Marsella et al., 2008), we calculate a conduit volume of 0.002 km^3, corresponding to about 25% of the total lava volume erupted (0.0088 km^3; Landi et al., 2006; Marsella et al., 2008). For a conduit length of about 2.5 km, a radius of 33 m, or a side of 30 m, can be calculated for a circle, or square, section conduit, respectively.

Furthermore, the total volume of erupted magma as lava flow can represent a proportion of about 3% or 20% of the volume of the reservoir according to the two magma chamber volume estimations reported in Francalanci et al. (1999) (0.3 or 0.04 km^3, respectively, depending on the different evaluations of magma input flux at Stromboli; Giberti et al., 1992; Allard et al., 1994; Harris and Stevenson, 1997). Although there is no real possibility to choose between the two estimated reservoir volumes, we guess more probable the smaller size, mainly based on the short time the bulk system takes to re-homogenise the composition (Francalanci, unpublished data). In this case, the erupted magma volume during lava effusion would represent a proportion of 20% and the estimated conduit volume is a proportion of about 5% of the total magma chamber volume.

In the end, according to the decrease of $^{87}Sr/^{86}Sr$ values of lava groundmass along the effusive event, we calculated that a total amount of 30% of LP-magma was arrived in the shallow HP-magma reservoir after the 5-April paroxysm. Thus, estimating a 70% of interstitial liquid in the magma reservoir (the crystallinity increases to about 50% along the conduit to the surface) and taking in mind the preferred estimation of magma chamber volume, we calculate at 0.0084 (0.04x0.7x0.3) km^3 the total volume of LP-magma input, which is intriguingly the same volume of the magma erupted as lava flows during the 2002-2003 event.

Acknowledgements

We sincerely thank Filippo Olmi for allowing access to EPMA facilities and for his skilful assistance during microprobe analyses. Mario Zaia (Zazà), Alpine guides of Stromboli and Soccorso Alpino of Guardia di Finanza from Nicolosi (Catania) are thanked for their field assistance during sampling. Chiara M. Petrone, Elena Boari and Simone Tommasini are warmly thanked for helping and sharing time during isotope analyses. Sandro Conticelli is thanked for constant encouragement and final critical reading. Funding was provided by Italian Civil Defence through INGV-GNV and the European Commission of Energy, Environment and Sustainable Development, through ERUPT project (EVG1-CT2002-00058).

References

Anders, E. and Grevesse, N., 1989. Abundances of the elements: meteoric and solar. Geochimica et Cosmochimica Acta **53**, 197-214.

Aiuppa A., Federico C., Giudice G., Giuffrida G., Guida R., Gurrieri S., Liuzzo M., Moretti R., Papale P., 2009. The 2007 eruption of Stromboli volcano: insights from real-time measurement of the volcanic gas plume CO_2/SO_2 ratio. Journal of Volcanology and Geothermal Research, 182, 221-230.

Aiuppa A., Federico C., 2004. Anomalous magmatic degassing prior to the 5th April 2003 paroxysm on Stromboli. Geophys. Res. Lett. 31, LI4607, doi: 10.1029/2004GL020458.

Allard, P., Carbonnelle, J., Métrich, N., Loyer, H. and Zettwoog, P., 1994. Sulphur output and magma degassing budget of Stromboli volcano. Nature, 368, 326-330.

Allard P., 2010. A CO2-rich gas trigger of explosive paroxysms at Stromboli basaltic volcano, Italy. Journal Volcanology and Geothermal Research, 189, 363-374.

Armienti P., Francalanci L., Landi P. (2007) - Textural effects of steady state behaviour of the Stromboli feeding system. Journal of Volcanology and Geothermal Researches, 160, 86-98.

Avanzinelli, R., Boari, E., Conticelli, S., Francalanci, L., Gualtieri, L., Perini, G., Petrone, C.M., Tommasini, S., Ulivi, M., 2005. High precision Sr, Nd, and Pb isotopic analyses using new generation Thermal Ionisation Mass Spectrometer ThermoFinnigan Triton-Ti®. Periodico di Mineralogia 74, 3, 147-166.

Barberi, F., Rosi, M., Sodi, A., 1993. Volcanic hazard assessment at Stromboli based on review of historical data. Acta Vulcanologica 3, 173-187.

Bence, A.E., Albee, A.L., 1968. Empirical correction factors for the electron microanalysis of silicates and oxides. J. Geol. 76, 382-402.

Bertagnini, A., Coltelli, M., Landi, P., Pompilio, M., Rosi, M., 1999. Violent explosions yield new insights into dynamics of Stromboli volcano. EOS 80, 635-636.

Bertagnini, A., Métrich, N., Francalanci, L., Landi, P., Tommasini, S., Conticelli, S., 2008. Volcanology and magma geochemistry of the present day activity: constraints on the feeding system. In: "The Stromboli Volcano – An Integrated Study of 2002-2003 Eruption", S. Calvari, S. Inguaggiato, G. Puglisi, M. Ripepe, M. Rosi (edts), American Geophysical Union – Geophysical Monograph Series, vol. 182, 19-37.

Bonaccorso, A., Cardaci, C., Coltelli, M., Del Carlo, P., Falsaperla, S., Panucci, S., Pompilio, M., Villari, L., 1996. Annual report of the world volcanic eruptions in 1993, Stromboli. Bull.Volcanic Eruptions 33, 7-13.

Bonaccorso, A., Calvari, S., Garfi, G., Lodato, L., Patane, D., 2003. Dynamics of the December 2002 flank failure and tsunami at Stromboli volcano inferred by volcanological and geophysical observations. Geophys. Res. Lett. 30 (18), doi:10.1029/2003GL017702.

Burton M.R., Mader H.M., Polacci M., 2007. The role of gas percolation in quiescent degassing of persistently active basaltic volcanoes. Earth and Planetary Science Letters, 264, 46-60.

Capaldi, G., Guerra, I., Lo Bascio, A., Luongo, G., Pece, R., Rapolla, A., Scarpa, R., Del Pezzo, E., Martini, M., Ghiara, M.R., Lirer, L., Munno, R., La Volpe, L., 1978. Stromboli and its 1975 eruption. Bull. Volcanol. 41, 259-285.

Carapezza M.L., Inguaggiato S., Brusca L., Longo M., 2004. Geochemical precursors of the activity of an open-conduit volcano: the Stromboli 2002–2003 eruptive events. Geophysical Research Letters, 31, L07620, doi:10.1029/2004GL019614.

Charlier, B.L.A., C. Ginibre, D. Morgan, G.M. Nowell, D.G. Pearson, J.P. Davidson, and C.J. Ottley (2006), Methods for the microsampling and high-precision analysis of strontium and rubidium isotopes at single crystal scale for petrological and geochronological applications. Chem. Geol., 232, 114-133.

Chouet, B., Dawson, P., Ohminato, T., Martini, M., Saccorotti, G., Giudicepietro, F., De Luca, G., Milana, G., Scarpa, R., 2003. Source mechanisms of explosions at Stromboli Volcano, Italy, determined from moment tensor inversions of very-long-period data. Journal of Geophysical Research 108 (B1), 2109, doi:10.1029/2002ID001919.

Colò L., Ripepe M., Baker D.R., Polacci M., 2010. Magma vesiculation and infrasonic activity at Stromboli open conduit volcano. Earth and Planetary Science Letters 292, 274-280.

Davidson, J.P. and Tepley III, F.J., 1997. Recharge in volcanic systems: evidence from Isotope Profiles of Phenocrysts. Science 275, 826-829.

Davidson, J.P., Morgan, D.J., Charlier, B.L.A., Harlou, R., Hora, J.M., 2007. Microsampling and Isotopic Analysis of Igneous rocks: implications for the study of magmatic system. Ann. Rev. Earth Planet. Sci. 35, 273-311.

Davidson, J.P., Tepley III, F.J., Palacs, Z. & Meffan-Main, S., 2001. Magma recharge, contamination and residence times revealed by in situ laser ablation isotopic analysis of feldspar in volcanic rocks. Earth and Planetary Science Letters 184, 427-442.

De Fino, M., La Volpe, L., Falsaperla, S., Frazzetta, G., Neri, G., Francalanci, L., Rosi, M., Sbrana, A., 1988. The Stromboli eruption of December 6, 1985-April 25, 1986: volcanological, petrological and seismological data. Rendiconti Soc. Italiana Mineral. Petrol. 43, 1021-1038.

Di Carlo, I., Pichavant, M., Rotolo, S. G., Scaillet, B., 2006. Experimental crystallization of a high-K arc basalt: the golden pumice, Stromboli volcano (Italy). J. Petrol., 47, 1317-1343.

Di Salvo S., 2010. "Pizzo Sopra la Fossa" volcanic activity at Stromboli: geochemical and isotopic data (in Italian). B.Sc. Thesis, Università degli Studi di Firenze, 74 pp.

Fornaciai A., Landi P., Armienti P., 2009. Dissolution/crystallization kinetics recorded in the 2002-2003 lavas of Stromboli (Italy). Bull. Volcanol., 71, 631-641, DOI 10.1007/s00445-008-0249-3.

Francalanci L., 1993. Mineral chemistry of Stromboli volcanics as indicator of magmatic processes. Acta Vulcanologica, 3, 99-113.

Francalanci, L., Barbieri, M., Manetti, P., Peccerillo, A, Tolomeo, L., 1988. Sr-isotopic systematics in volcanic rocks from the island of Stromboli (Aeolian arc). Chem. Geol. 73, 164-180.

Francalanci L., Bertagnini A., Métrich N., Renzulli A., Vannucci R., Landi P., Del Moro S., Menna M., Petrone C.M., Nardini I. 2008. Mineralogical, geochemical and isotopic characteristics of the ejecta from the 5 April 2003 paroxysm at Stromboli, Italy: inferences on the pre-eruptive magma dynamics. In: "The Stromboli Volcano – An Integrated Study of 2002-2003 Eruption", S. Calvari, S. Inguaggiato, G. Puglisi, M. Ripepe, M. Rosi (edts), American Geophysical Union – Geophysical Monograph Series, vol. 182, 331-345.

Francalanci L., Davies G.R., Lustenmhower W., Tommasini S., Mason P.R.D., Conticelli S., 2005. Old crystal re-cycle and multiple magma reservoirs in the plumbing system of the present day activity at Stromboli volcano, South Italy: Sr-isotope in situ microanalyses. J. Petrol. 46, 1997-2021. doi: 10.1093/petrology/egi045.

Francalanci, L., Manetti, P., Peccerillo, A., 1989. Volcanological and magmatological evolution of Stromboli volcano (Aeolian islands): the roles of fractional crystallisation, magma mixing, crustal contamination and source heterogeneity. Bull. Volcanol. 51, 355-378.

Francalanci, L., Manetti, P., Peccerillo A., Keller, J., 1993. Magmatological evolution of the Stromboli volcano (Aeolian Arc, Italy): inferences from major and trace element and Sr-isotopic composition of lavas and pyroclastic rocks. Acta Vulcanol. 3, 127-151.

Francalanci, L., Tommasini, S., Conticelli, S., 2004. The volcanic activity of Stromboli in the 1906-1998 period: mineralogical, geochemical and isotope data relevant to the understanding of Strombolian activity. J. Volcanol. Geoth. Res. 131, 179-211.

Francalanci, L., Tommasini, S., Conticelli, S., Davies, G.R., 1999. Sr isotope evidence for short magma residence time for the 20th century activity at Stromboli volcano, Italy. Earth Planet. Sci. Lett. 167, 61-69.

Giberti, G., Jaupart, C. and Sartoris, G. (1992). Steady-state operation of Stromboli volcano, Italy: constraints on the feeding system. Bulletin of Volcanology 54, 535-541.

Gillot, P.Y., Keller, J., 1993. Radiochronological dating of Stromboli. Acta Vulcanologica 3: 69-77.

Harris, A.J.L., Ripepe, M., Calvari, S., Lodato, L., Spampinato, L., 2008. The 5 April 2003 explosion of Stromboli: timing of eruption dynamics using thermal data. In: "The Stromboli Volcano – An Integrated Study of 2002-2003 Eruption", S. Calvari, S. Inguaggiato, G. Puglisi, M. Ripepe, M. Rosi (edts), American Geophysical Union – Geophysical Monograph Series, vol. 182, 305-316.

Harris, A.J.L. and Stevenson, D.S. (1997). Magma budgets and steady state activity of Vulcano and Stromboli. Geophysical Research Letters 24, 1043-1046.

Hornig-Kjarsgaard, I., Keller, J., Koberski, U., Stadlbauer, E., Francalanci, L., Lenhart, R., 1993. Geology, stratigraphy and volcanological evolution of the island of Stromboli, Aeolian arc, Italy. Acta Vulcanologica 3, 21-68.

Keller, J., Hornig-Kjarsgaard, I., Koberski, U., Stadlbauer, E., Lenhart, R., 1993. Geological map of the island of Stromboli – scale 1:10,000. Acta Vulcanologica 3, appendix.

Kokelaar, P. & Romagnoli, C., 1995. Sector collapse, sedimentation and clast population evolution at an active island-arc volcano: Stromboli, Italy. Bulletin of Volcanology **57**, 240-262.

Landi P., Corsaro R.A., Francalanci L., Civetta L., Miraglia L., Pompilio M., Tesoro R., 2009. Magma dynamics during the 2007 Stromboli eruption (Aeolian Islands. Italy) : mineralogical, geochemical and isotopic data. J. Volcanol. Geoth. Res., 182, 255-268.

Landi, P., L. Francalanci, M. Pompilio, M. Rosi, R.A. Corsaro, C.M. Petrone, I. Cardini, and L. Miraglia L., 2006. The December 2002–July 2003 effusive event at Stromboli volcano, Italy: Insights into the shallow plumbing system by petrochemical studies, *J. Volcanol. Geotherm. Res., 155*, 263-284.

Landi P., Francalanci L., Corsaro R.A., Petrone C.M., Fornaciai A., Carroll M., Nardini I., Miraglia L.. 2008. Textural and compositional characteristics of the lavas erupted in the December 2002-July 2003 effusive events at Stromboli, Aeolian Island, Italy. In: "The Stromboli Volcano – An Integrated Study of 2002-2003 Eruption", S. Calvari, S. Inguaggiato, G. Puglisi, M. Ripepe, M. Rosi (edts), American Geophysical Union – Geophysical Monograph Series, vol. 182, 213-228.

Landi, P., Métrich, N., Bertagnini, A., Rosi, M., 2004. Dynamics of magma mixing and degassing recorded in plagioclase at Stromboli (Aeolian Arcipelago, Italy). Contrib. Mineral. Petrol. 147, 213-227.

Lautze N.C., Houghton B.F., 2007. Linking variable explosion style and magma textures during 2002 at Stromboli volcano, Italy. Bull. Volcanol., 69, 445-460, DOI 10.1007/s00445-006-0086-1.

Marsella, M., Coltelli, M., Proietti, C., Branca, S., Monticelli, R., 2008. 2002-2003 lava flow eruption of Stromboli: a contribution to understanding lava discharge mechanisms using periodic digital photogrammetry surveys. In: "The Stromboli Volcano – An Integrated Study of 2002-2003 Eruption", S. Calvari, S. Inguaggiato, G. Puglisi, M. Ripepe, M. Rosi (edts), American Geophysical Union – Geophysical Monograph Series, vol. 182, 229-246.

Métrich N., Bertagnini A., Landi P., Rosi, M., 2001. Crystallization driven by decompression and water loss at Stromboli volcano (Aeolian Islands, Italy). J. Petrol. 42, 1471-1490.

Métrich, N., Bertagnini, A., Landi, P., Rosi, M., 2005. Triggering mechanism at the origin of paroxysms at Stromboli (Aeolian Arcipelago, Italy): The 5 April 2003 eruption. Geophys. Res. Lett. 32, L10305, doi:10.1029/2004GL022257.

Metrich, N., Bertagnini, A., Di Muro, A., 2010. Conditions of magma storage, degassing and ascent at Stromboli: new insights into the volcano plumbing system with inferences on the eruptive dynamics. J. Petrol., 51, 603-626.

Morelli, C., Giese, P., Cassinis, R., Colombi, B., Guerra, I., Luongo, G., Scarascia, S., Shutte, K.G., 1975. Crustal structure of Southern Italy. A seismic refraction profile between Puglia-Calabria-Sicily. Boll. Geofisica Teorica Applicata 18, 183-210.

Pasquarè, G., Francalanci, L., Garduño, V.H., Tibaldi, A., 1993. Structure and geologic evolution of the Stromboli volcano, Aeolian islands, Italy. Acta Vulcanologica 3, 79-89.

Perini, G., Tepley III, F.J., Davidson, J.P. and Conticelli, S. (2003). The origin of K-feldspar megacrysts hosted in alkaline potassic rocks from central Italy: a track for low-pressure processes in mafic magmas. Lithos 66, 223-240.

Petrone C.M., Francalanci L., Braschi E., 2004. Pyroclastic deposits associated with sector collapses at Stromboli volcano: inferences from mineralogical, geochemical and isotopic data. Italia 2004, 32° International Geological Congress, Firenze, Abstracts, Part 1, 68-20, pag. 334.

Petrone C.M., Olmi F., Braschi E., Francalanci L., 2006. Mineral chemistry profile: a valuable

approach to unravel magma mixing processes in the recent volcanic activity of Stromboli, Italy. Periodico di Mineralogia, 75, 2-3, 277-292.

Pistolesi, M., Rosi M., Pioli L., Renzulli A., Bertagnini A., Andronico D., 2008. The paroxysmal explosion and its deposits. In: "The Stromboli Volcano – An Integrated Study of 2002-2003 Eruption", S. Calvari, S. Inguaggiato, G. Puglisi, M. Ripepe, M. Rosi (edts), American Geophysical Union – Geophysical Monograph Series, vol. 182, 317-330.

Puglisi, G., Bonaccorso, A., Mattia, M., Aloisi, M., Bonforte, A., Campisi, O., Cantarero, M., Falzone, G., Puglisi, B., Rossi, M., 2005. New integrated geodetic monitoring system at Stromboli volcano (Italy). Engineering Geology 79, 13-31.

Ramos, F.C., Wolff, J.A. and Tollstrup, D.L., 2004. Measuring $^{87}Sr/^{86}Sr$ variations in minerals and groundmass from basalts using LA-MC-ICPMS. Chemical Geology, 211, 135-158.

Ripepe, M., Delle Donne D., Harris, A.J.L., Marchetti, E., Ulivieri, G., 2008. Dynamics of Strombolian activity. In: "The Stromboli Volcano – An Integrated Study of 2002-2003 Eruption", S. Calvari, S. Inguaggiato, G. Puglisi, M. Ripepe, M. Rosi (edts), American Geophysical Union – Geophysical Monograph Series, vol. 182, 39-48 [doi: 10.1029/182GM05].

Ripepe, M., Harris, A.J.L., Carniel, R., 2002. Thermal, seismic and infrasonic evidences of variable degassing rates at Stromboli volcano. J. Volcanol. Geoth. Res. 118, 285-297.

Ripepe, M., Marchetti, E., Ulivieri, G., Harris, A., Dehn, J., Burton, M., Caltabiano, T. and Salerno, G., 2005. Effusive to explosive transition during the 2003 eruption of Stromboli volcano. Geology 33(5), 341-344.

Rosi, M., A. Bertagnini, A.J.L. Harris, L. Pioli, M. Pistolesi, and M. Ripepe, 2006. A case history of paroxysmal explosion at Stromboli: Timing and dynamics of the April 5, 2003 event, Earth and Planet. Sci. Lett., 243, 3-4, 594-606, 2006.

Rosi, M., Bertagnini, A., Landi, P., 2000. Onset of the persistent activity at Stromboli volcano (Italy). Bull. Volcanol. 62, 294-300.

Schiavi, F., Kobayashi, K., Moriguti, T., Nakamura, E., Pompilio, M., Tiepolo, M., Vannucci, R., 2010. Degassing, crystallization and eruption dynamics at Stromboli: trace element and lithium isotopic evidence from 2003 ashes. Contrib.Mineral. Petrol., 159, 541-561.

Spampinato, L., Calvari, S., Harris, A.J.L., Dehn, J., 2008. Evolution of the lava flow field by daily thermal and visible airborne surveys. In: "The Stromboli Volcano – An Integrated Study of 2002-2003 Eruption", S. Calvari, S. Inguaggiato, G. Puglisi, M. Ripepe, M. Rosi (edts), American Geophysical Union – Geophysical Monograph Series, vol. 182, 201-212.

Speranza, F., Pompilio, M., D'Ajello Caracciolo, F. and Sagnotti, L., 2008. Holocene eruptive history of the Stromboli volcano: Constraints from paleomagnetic dating. Journal of Geophysical Research, 113, doi:10.1029/2007JB005139.

Tepley III, F.J. and Davidson, J.P. (2003). Mineral-scale Sr-isotope constraints on magma evolution and chamber dynamics in the Rum layered intrusion, Scotland. Contribution to Mineralogy and Petrology, 145, 628-641.

Tepley III, F.J., Davidson, J.P. and Clynne, M.A. (1999). Magmatic interactions as recorded in Plagioclase phenocrysts of Chaos Crags, Lassen Volcanic Center, California. Journal of Petrology, 40, 787-806.

Tepley III, F.J., Davidson, J.P., Tilling, R.I. and Arth, J.G. (2000). Magma mixing, Recharge and Eruption Histories Recorded in Plagioclase Phenocrysts from El Chichòn Volcano, Mexico. Journal of Petrology, 41, 1397-1411.

Thirlwall, M.F., 1991. Long-term reproducibility of multicollector Sr and Nd ratio analyses. Chem. Geol. 94, 85-104.

Tibaldi, A., 2001. Multiple sector collapses at Stromboli volcano: how they work. Bull. Volcanol. 63, 112-125.

Tommasi, P., Baldi, P., Chiocci, F.L., Coltelli, M., Marsella, M., Pompilio, M., Romagnoli C., 2005. The landslide sequence induced by the 2002 eruption at Stromboli volcano. In: Landslide - Risk analysis and sustainable disaster management, chapter 32: 251-258, Springer Verlag.

Tommasi, P., Chiocci, F.L., Marsella, M., Coltelli, M., Pompilio, M., 2004. Preliminary analysis of the December 2002 instability phenomena at Stromboli volcano., in Occurence and mechanisms of flow-like landslides in natural slopes and earthfills, Sorrento, pp. 297-303.
Vaggelli, G., Francalanci, L., Ruggieri, G., Testi, S., 2003. Persistent polybaric rests of calc-alkaline magmas at Stromboli volcano, Italy: pressure data from fluid inclusions in restitic quartzite nodules. Bull. Volcanol. 65, 385-404
Vaggelli, G., Olmi, F., Conticelli, S., 1999. Evaluation of analytical errors during microprobe analyses of silicate minerals international reference samples. Acta Vulcanologica 11, 297-303.
Wolff, J.A., Ramos, F.C. and Davidson, J.P. (1999). Sr isotope disequilibrium during differentiation of the Bandelier Tuff: constraints on the crystallisation of a large rhyolitic magma chamber. Geology 27, 495-498.

TABLE CAPTIONS

Table 1 – Trace element contents and compositional end-members in the clinopyroxene crystals analysed for micro-Sr isotope ratios, from the 2002-2003 Stromboli products. En: Enstatite, Fs: Ferrosilite, Wo: Wollastonite, Mg# [molar $Mg^{2+}/(Mg^{2+}+Fe^{2+})$]: Mg-value; "-": below detection limits; nd: not determined; N: Chondrite-normalised (Anders and Grevesse, 1989).

Table 2a,b – Trace element contents and compositional end-members in the plagioclase crystals, analysed for micro-Sr isotope ratios, from the 2002-2003 Stromboli products. "-": below detection limits; nd: not determined. An: Anorthite, Ab: Albite, Or: Orthoclase, Cn: Celsia; N: Chondrite-normalised (Anders and Grevesse, 1989).

Table 3 – Sr isotope ratios in whole-rocks, groundmasses and minerals (micro-drilled and separated) from the 2002-2003 Stromboli products. L: lenght of crystal, DEPTH: depth of drilling, TRACE: zones analysed for trace elements. Asterisks + italics: data from Landi et al., (2006). C: core, OC: outer core, IR: inner rim, R: rim, OR: outer rim; numbers in brackets indicate anorthite content and Mg# [molar $Mg^{2+}/(Mg^{2+}+Fe^{2+})$] for plagioclase and clinopyroxene, respectively. "-": no significant or available data. All the data from microdrilling are those with reported DEPTH.

Table ESM-1 – Electron microprobe analyses of the clinopyroxene micro-milled for Sr isotope data. Mg# [molar $Mg^{2+}/(Mg^{2+}+Fe^{2+})$]: Mg-value; En: Enstatite, Fs: Ferrosilite, Wo: Wollastonite; bdl: below detection limits (0.01 wt%, Vaggelli et al., 1999)

Table ESM-2 – Electron microprobe analyses of plagioclase micro-milled for Sr isotope data. Numbers in italics: not drilled zone for Sr isotopes; An: anorthite, Ab: albite, Or: orthoclase, Cn: Celsian; bdl: below detection limits (0.01 wt%, Vaggelli et al., 1999)

FIGURE CAPTIONS

Fig. 1 - Simplified geological map of the emerged Stromboli volcano with reported the 2002-2003 lava setting along the Sciara del Fuoco scar. P: Pianoro; Pizzo: Pizzo Sopra la Fossa. For each legend-box, the referred eruptive period (Paleostromboli, Vancori, Neostromboli, Recent), the age in ka, the magmatic series (CA: calc-alkaline, HKCA: high-K calc-alkaline, SHO: shoshonitic, KS: potassic) and the range of Sr isotope ratios of the erupted magmas for each period are reported (data from Francalanci et al., 1988, 1993, 1999, 2004, 2005; Hornig-Kjarsgaard et al., 1993; Gillot and Keller, 1993; Rosi et al., 2000; Speranza et al., 2008 and Di Salvo, 2010); a: craters, b: eruptive fissure, c: sector collapse, d: caldera collapse. Map modified after Keller et al. (1993) and Tibaldi (2001).
Inset on the left top: bathymetric map of the Aeolian volcanic arc (Southern Tyrrhenian Sea, Italy) showing the Stromboli location. The name of the other main islands (in grey colour) is also reported.

Fig. 2 – Scanner image of a polished thin section (60 μm thick) from the 28-December-2002 lava sample (STR1202a) (onset lavas), with enlarged pictures of the minerals micro-drilled for Sr isotope ratios. The name of the analysed minerals is reported on each picture (Pl: plagioclase, Cpx: clinopyroxene). The section shows phenocrysts and microphenocrysts of clinopyroxene (green and large crystals), olivine (pale, clear, fractured and large crystals) and plagioclase (pale, sieved and zoned crystals) included in a dark glassy groundmass. The coloured areas on the enlarged minerals show the crystal zones micro-milled for Sr isotope analyses on each mineral. The obtained $^{87}Sr/^{86}Sr$ value for each micro-milled zone is also reported in white colour. The two blue areas of Cpx13 and the two external blue areas of Pl2 are collected in two single micro-samples, respectively. The general mineral zones recognised are reported in yellow (C: core, OC: outer-core, IR: inner-rim, R: rim, OR: outer-rim) together with the An content (wt%) of plagioclase and the Mg# [mole Mg/(Mg+Fe)] of clinopyroxene for each zone when available. The white spots in Pl2, Cpx13 and Pl4 indicate LAM-ICP-MS analyses.

Fig. 3 – Core to outer-rim variation of anorthite contents in some plagioclases micro-drilled for Sr isotope analyses (the name of plagioclase is reported for each crystal) from the different samples collected during the 2002-2003 effusive event. Each figure is referred to a sample from a product erupted in the relative date reported. C: core, OC: outer-core, IR: inner-rim, R: rim, OR: outer-rim.

Fig. 4 – Sr isotope ratios of whole-rocks (full symbols) and groundmasses (gdm; blue open symbol) versus time for the products erupted during the effusive event (28-December-2002 – 22-July-2003) and the paroxysm (5-April-2003). Only the groundmass with written "scoria" is referred to a scoria groundmass (erupted by 5-April paroxysm), the other blue open symbols are referred to lava groundmass. The Sr isotope ratios of separated single crystals of olivine and plagioclase from the sample of lavas erupted on 14-April-2003 (STR140403), are also reported. As indicated in the figure, the coloured fields report the isotopic compositional variation of pumices (yellow: LP-magma) erupted between years 1996-2000 and scoria (blue: HP-magma) erupted between years 1994-1999 and 2001-June 2002. The 2000 scoria have a higher $^{87}Sr/^{86}Sr$ up to 0.70620. Scoria and lavas erupted before 1994 and during the entire 20th century have higher $^{87}Sr/^{86}Sr$ up to 0.70626 (data of fields are from Francalanci et al., 1999, 2004, 2005 and unpublished).

Fig. 5 – (a) Micro-Sr isotope ratios for core-rim traverses in clinopyroxene (Cpx: triangles) and plagioclase (Pl: squares) of the 28-December-2002 lava sample (name: STR1202a). Sr isotope data on a separated clinopyroxene crystal (asterisk), on whole-rocks (full circle) and groundmasses (open circle) (separated and drilled, Table 3a) are also reported. Legend of the core-rim traverse of minerals: full violet-squares = crystal cores, full blue-squares and green triangle =

intermediate zones of crystals; open light-violet-squares = prevalent outer-rims. C: core, OC: outer-core, IR: inner-rim, R: rim, OR: outer-rim. Numbers in parentheses indicate the Mg# [mole Mg/(Mg+Fe)] of clinopyroxene and the An% of plagioclase for the referred crystal zone. Pl2, Pl4 and Cpx13 are crystals also analysed for trace elements by LAM-ICP-MS and reported in Figure 5b,c,d. **(b, c, d)** Chondrite-normalised (Anders and Grevesse, 1989) trace element patterns for plagioclase (b: Pl2, c: Pl4) and clinopyroxene (d: Cpx13) of the 28 December 2002 lava sample. An% for plagioclase and Mg# for clinopyroxene of the analysed zones are also given in parentheses in the legends. Element ordering: REE have been reported separately from the other elements, which are in order of increasing compatibility into a basaltic mineral assemblage.

Fig. 6 – Micro-Sr isotope ratios for core-rim traverses in clinopyroxene (Cpx) and plagioclase (Pl) of the 06-March-2003 lava sample (names: STR060303 and STR040303 for whole-rock) **(a)** and 13-May-2003 lava sample (name: STR130503) **(b)**. Sr isotope data on a separated clinopyroxene crystal (asterisk), on whole-rocks (full circle) and groundmasses (open circle) (separated and drilled, Table 3a,b) are also reported. Legend of the core-rim traverse of minerals: full violet-squares = crystal cores, full blue-squares = intermediate zones of crystals; open light-violet-squares = prevalent outer-rims. C: core, OC: outer-core, IR: inner-rim, R: rim, OR: outer-rim. When available, the numbers in parentheses indicate the An% of plagioclase for the referred crystal zone.

Fig. 7 – **(a)** Micro-Sr isotope ratios for core-rim traverses in clinopyroxene (Cpx: triangles) and plagioclase (Pl: squares) of the 5-April-2003 pumice (yellow area) and scoria (white area) samples (names: STR050403hP, STR050403hS and STR050403f, respectively). Sr isotope data on a separated olivine (Olv) crystal (cross), on whole-rock (full circle) and separated groundmasses (open circle) are also reported. Legend of the core-rim traverse of minerals: full violet-squares = crystal cores, full blue-squares = intermediate zones of crystals; open green-triangle = prevalent outer rims. C: core, OC: outer-core, IR: inner-rim, R: rim, OR: outer-rim. Numbers in parentheses indicate the Mg# [mole Mg/(Mg+Fe)] of clinopyroxene and the An% of plagioclase for the referred crystal zone. Pl1, Pl3, Pl1hS, Pl2hP and Cpx1 are crystals also analysed for trace elements by LAM-ICP-MS and reported in Figure 7b,c,d,e. **(b, c, d, e)** Chondrite-normalised (Anders and Grevesse, 1989) trace element patterns for plagioclase (b: Pl1hS, c: Pl1, Pl3, d: Pl2hP) and clinopyroxene (e: Cpx1) of the 5 April 2003 pumice (yellow area) and scoria (white areas) samples. An% for plagioclase of the analysed zones are also given in parentheses in the legends. Element ordering: REE have been reported separately from the other elements, which are in order of increasing compatibility into a basaltic mineral assemblage.

Fig. 8 – **(a)** Micro-Sr isotope ratios for core-rim traverses in clinopyroxene (Cpx: triangles) and plagioclase (Pl: squares) of the 17-May-2003 lava sample (name: STR170503). Sr isotope data on separated clinopyroxene and olivine (Olv) crystals (asterisk and cross, respectively), on whole-rock (full circle) and drilled groundmass (open circle) are also reported. Legend of the core-rim traverse of minerals: full violet-squares and green-triangle = crystal cores, full blue-squares = intermediate zones of crystals; open green triangle = outer rim. C: core, OC: outer-core, IR: inner-rim, R: rim, OR: outer-rim. Numbers in parentheses indicate the Mg# [mole Mg/(Mg+Fe)] of clinopyroxene and the An% of plagioclase for the referred crystal zone. Pl2, Pl2, Pl3 and Cpx2 are crystals also analysed for trace elements by LAM-ICP-MS and reported in Figure 8b,c,d,e. **(b, c, d, e)** Chondrite-normalised (Anders and Grevesse, 1989) trace element patterns for plagioclase (b: Pl1, c: Pl2, d: Pl3) and clinopyroxene (e: Cpx2) of the 17 May 2003 lava sample. An% for plagioclase and Mg# for clinopyroxene of the analysed zones are also given in parentheses in the legends. Element ordering: REE have been reported separately from the other elements, which are in order of increasing compatibility into a basaltic mineral assemblage.

Fig. 9 – **(a)** Micro-Sr isotope ratios for core-rim traverses in plagioclase (Pl: squares) of the 20-July-2003 lava sample (name: STR200703). Sr isotope data on a separated clinopyroxene (Cpx) crystal (asterisk), on whole-rock (full circle) and separated groundmass (open circle) are also reported. Legend of the core-rim traverse of minerals: full violet-squares = crystal cores, full blue-squares = intermediate zones of crystals; open light-violet-squares = prevalent outer rims. C: core, OC: outer-core, IR: inner rim, R: rim, OR: outer-rim. Numbers in parentheses indicate the An% of plagioclase for the referred crystal zone. Pl1 and Pl2 are crystals also analysed for trace elements by LAM-ICP-MS and reported in Figure 9b,c. **(b, c)** Chondrite-normalised (Anders and Grevesse, 1989) trace element patterns for plagioclase (b: Pl1 c: Pl2) of the 20 July 2003 lava sample. An% for plagioclase of the analysed crystal zones are also given in parentheses in the legends. Element ordering: REE have been reported separately from the other elements, which are in order of increasing compatibility into a basaltic mineral assemblage.

Fig. 10 – Comparison of clinopyroxene (a) and plagioclase (b) compositions between the 2002-2003 products (data from the present paper and unpublished) and the other rocks of Stromboli belonging to the different magmatic series (CA: calc-alkaline, HKCA: high-K calc-alkaline, SHO: shoshonitic, KS: potassic series). (a) Sr versus La and Zr contents for clinopyroxene and (b) Anorthite content (An%) versus K_2O (wt%) for plagioclase in the different Stromboli magmas. These figures show a shoshonitic composition for clinopyroxene and plagioclase of the 2002-2003 products. Font of comparison data: the trace element contents of clinopyroxene are our unpublished data, whereas the plagioclase composition is from Francalanci (1993).

Fig. 11 – **(a)** Micro-Sr isotope ratios for core-rim traverses in clinopyroxene (triangles) and plagioclase (squares) of all the analysed 2002-2003 lava samples. Sr isotope data on separated clinopyroxene and olivine crystals (asterisks and crosses, respectively), on whole-rocks (full circles) and groundmasses (open circles) are also reported. The error bars are included in the symbol size. More detailed legends are reported in Figures 5-9. Each figure is referred to a sample from a product erupted in the relative date reported. The horizontal line indicates the Sr isotope ratio of the groundmass for each sample.

Fig. 12 – Cartoon of the intermediate plumbing system (HP-magma reservoir and crystal mush zone) feeding the present-day activity of Stromboli during the 2002-2003 eruptive crisis. Based on the data reported in this paper, the picture represents an interpretative model of the shallow HP-magma reservoir and its relationship with a cumulus crystal mush zone sited below. Some significant crystal zoning, effectively found in the specified minerals, are schematically drawn as examples (letters indicate the drilled crystal-zones, C: core, OC: outer-core, IR: inner rim, R: rim, OR: outer-rim). It is considered that a significant amount of LP-magmas arrived (before and possibly after the onset of the lava flow and during the 5-April paroxysm) and mixed in the shallow HP-magma reservoir, passing through a cumulus crystal mush zone, formed since the "Pizzo Sopra la Fossa" activity (about 2.5 ka ago), and carrying high Sr-isotope antecrysts (grey squares) in the reservoir. High Sr-isotope antecrysts (blue squares) also form by the dynamic processes of the Strombolian activity, when descending degassed HP-magma sinks in the lower magmas and are re-cycled by convective movements. $^{87}Sr/^{86}Sr$ values of the different crystals, crystal zones, antecrysts and interstitial liquids are also written in figure. Other explanations are reported in the figure and in the text. The crystal size, the conduit width and length are not in scale. The relative aspect ratios of the HP-magma reservoir and crystal mush are hypothetical.

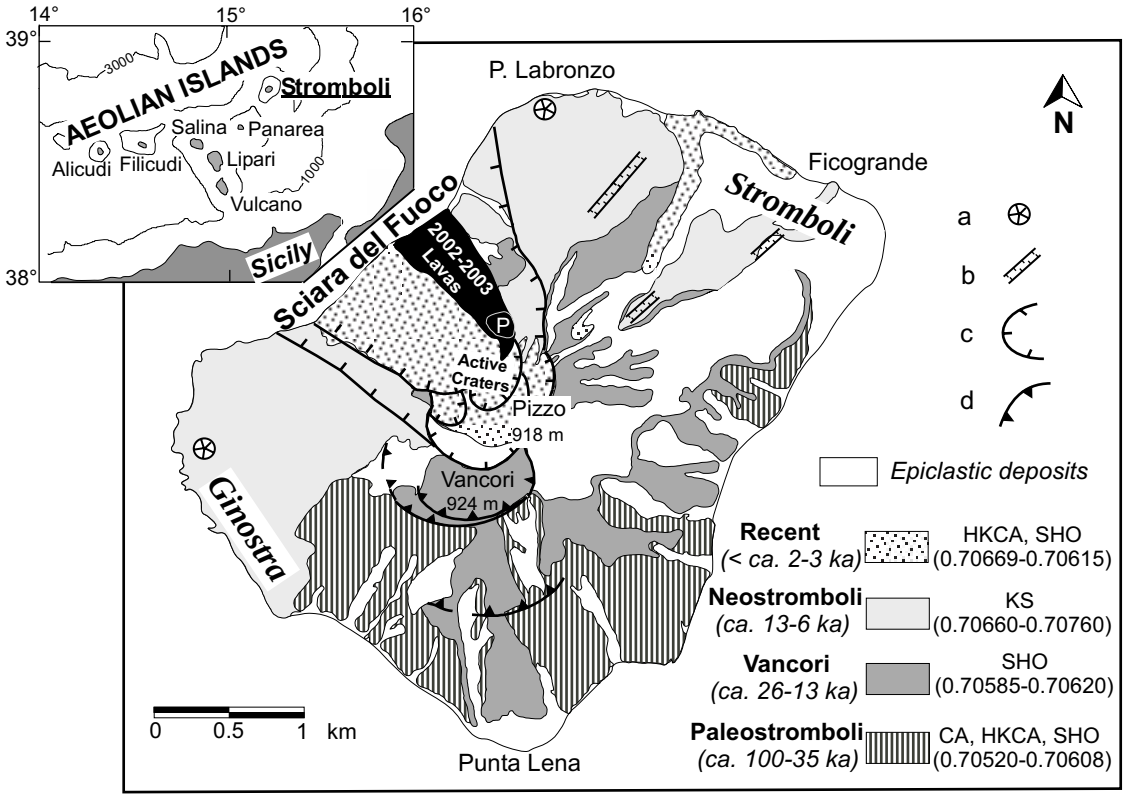
14°
15°
16°
39°
38°
AEOLIAN ISLANDS
Stromboli
Salina
Panarea
Alicudi
Filicudi
Lipari
Vulcano
Sicily
3000
1000
P. Labronzo
Ficogrande
Stromboli
Sciara del Fuoco
2002-2003 Lavas
P
Active Craters
Pizzo
918 m
Vancori
924 m
Ginostra
Punta Lena
N
a
b
c
d
Epiclastic deposits
Recent
(< ca. 2-3 ka)
HKCA, SHO
(0.70669-0.70615)
Neostromboli
(ca. 13-6 ka)
KS
(0.70660-0.70760)
Vancori
(ca. 26-13 ka)
SHO
(0.70585-0.70620)
Paleostromboli
(ca. 100-35 ka)
CA, HKCA, SHO
(0.70520-0.70608)
0
0.5
1
km

Fig. 1

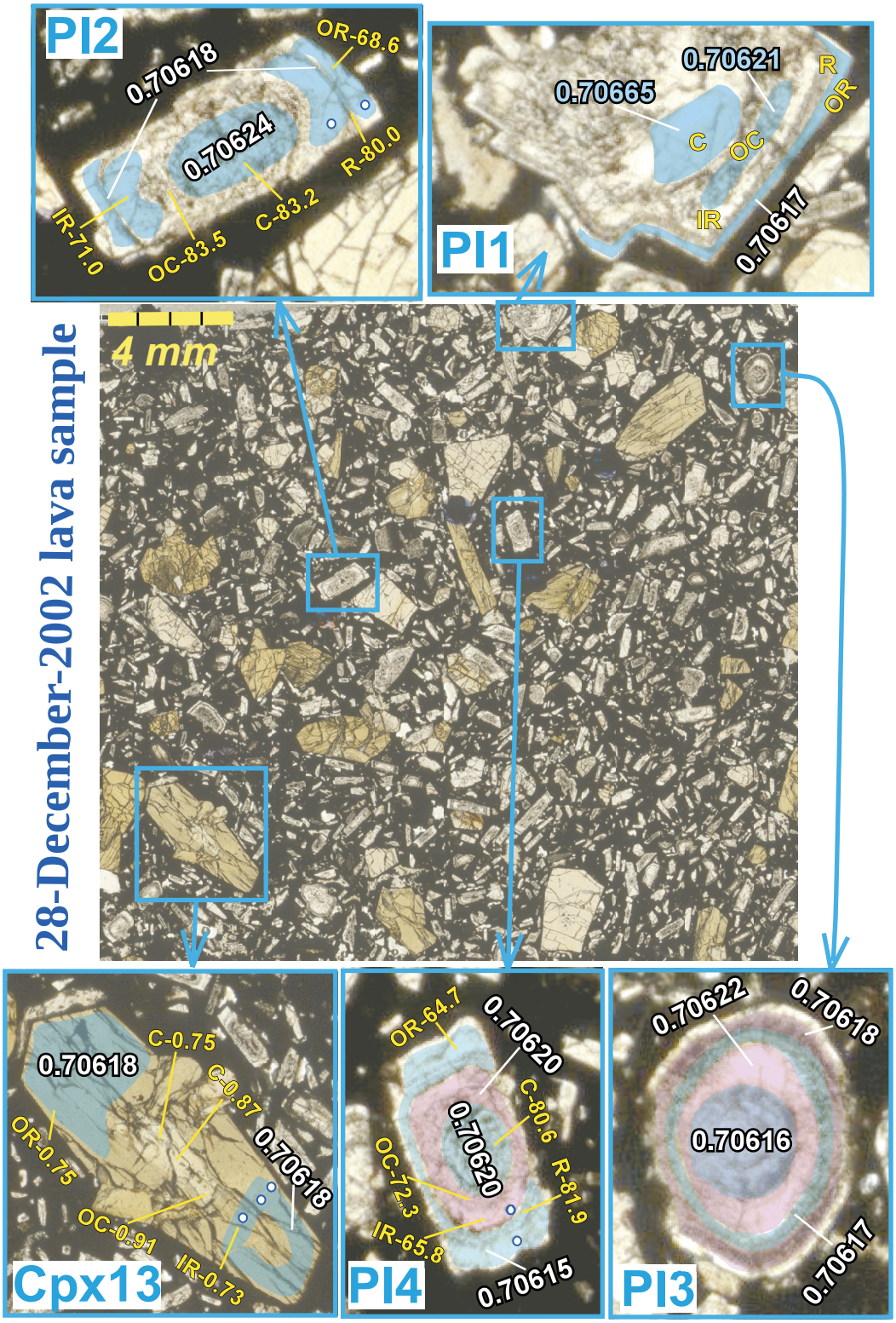
PI2
0.70618
OR-68.6
0.70624
R-80.0
C-83.2
IR-71.0
OC-83.5
PI1
0.70621
R
OR
0.70665
C
OC
IR
0.70617
4 mm
28-December-2002 lava sample
Cpx13
0.70618
C-0.75
C-0.87
0.70618
OR-0.75
OC-0.91
IR-0.73
PI4
OR-64.7
0.70620
C-80.6
0.70620
OC-72.3
R-81.9
IR-65.8
0.70615
PI3
0.70622
0.70618
0.70616
0.70617

Fig. 2

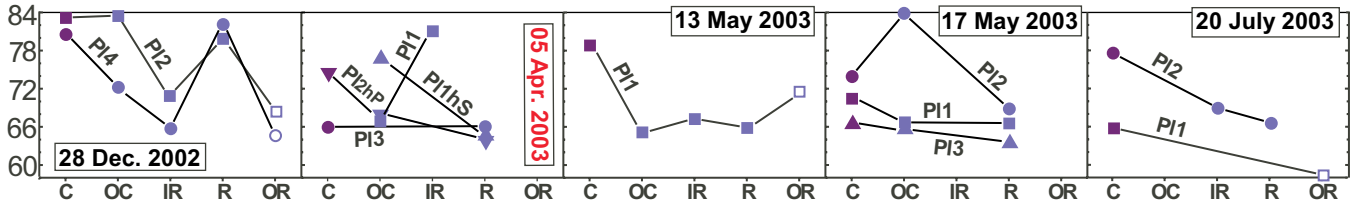
84
78
72
66
60
C OC IR R OR
28 Dec. 2002
Pl4
Pl2
Pl2hP
Pl1
Pl1hS
Pl3
05 Apr. 2003
13 May 2003
Pl1
17 May 2003
Pl2
Pl1
Pl3
20 July 2003
Pl2
Pl1

Fig. 3

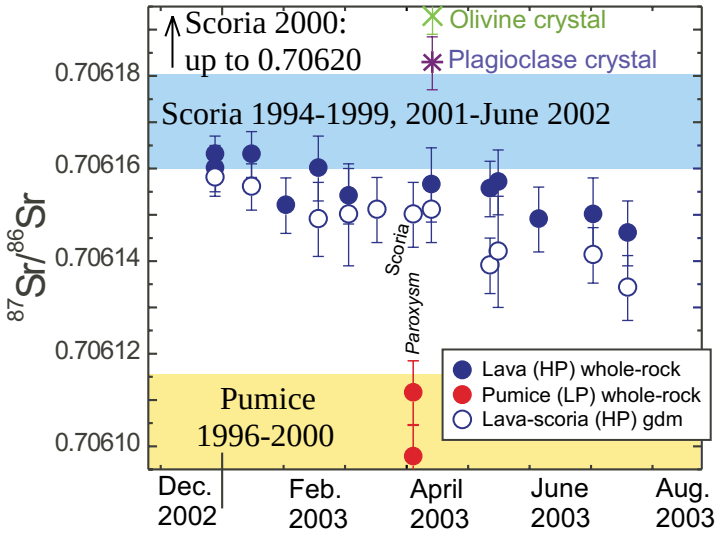
Scoria 2000:
up to 0.70620
Olivine crystal
Plagioclase crystal
Scoria 1994-1999, 2001-June 2002
Pumice
1996-2000
Scoria
Paroxysm
Lava (HP) whole-rock
Pumice (LP) whole-rock
Lava-scoria (HP) gdm
87Sr/86Sr
0.70618
0.70616
0.70614
0.70612
0.70610
Dec.
2002
Feb.
2003
April
2003
June
2003
Aug.
2003

Fig. 4

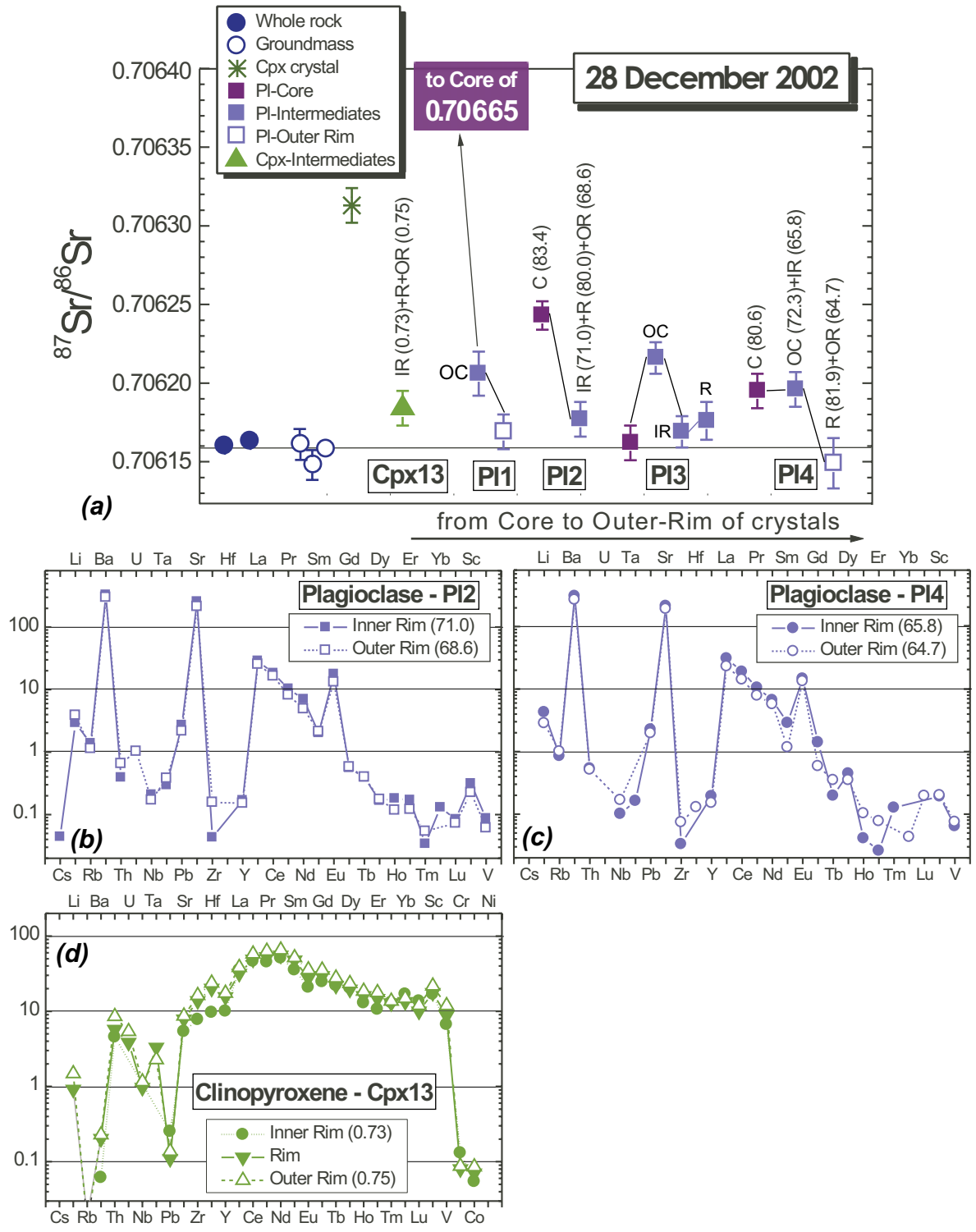
Whole rock
Groundmass
Cpx crystal
Pl-Core
Pl-Intermediates
Pl-Outer Rim
Cpx-Intermediates
to Core of
0.70665
28 December 2002
0.70640
0.70635
0.70630
0.70625
0.70620
0.70615
87Sr/86Sr
IR (0.73)+R+OR (0.75)
OC
C (83.4)
IR (71.0)+R (80.0)+OR (68.6)
OC
R
IR
C (80.6)
OC (72.3)+IR (65.8)
R (81.9)+OR (64.7)
Cpx13
Pl1
Pl2
Pl3
Pl4
(a)
from Core to Outer-Rim of crystals
Li Ba U Ta Sr Hf La Pr Sm Gd Dy Er Yb Sc
Plagioclase - Pl2
Inner Rim (71.0)
Outer Rim (68.6)
100
10
1
0.1
(b)
Cs Rb Th Nb Pb Zr Y Ce Nd Eu Tb Ho Tm Lu V
Li Ba U Ta Sr Hf La Pr Sm Gd Dy Er Yb Sc
Plagioclase - Pl4
Inner Rim (65.8)
Outer Rim (64.7)
(c)
Cs Rb Th Nb Pb Zr Y Ce Nd Eu Tb Ho Tm Lu V
Li Ba U Ta Sr Hf La Pr Sm Gd Dy Er Yb Sc Cr Ni
100
10
1
0.1
(d)
Clinopyroxene - Cpx13
Inner Rim (0.73)
Rim
Outer Rim (0.75)
Cs Rb Th Nb Pb Zr Y Ce Nd Eu Tb Ho Tm Lu V Co

Fig. 5

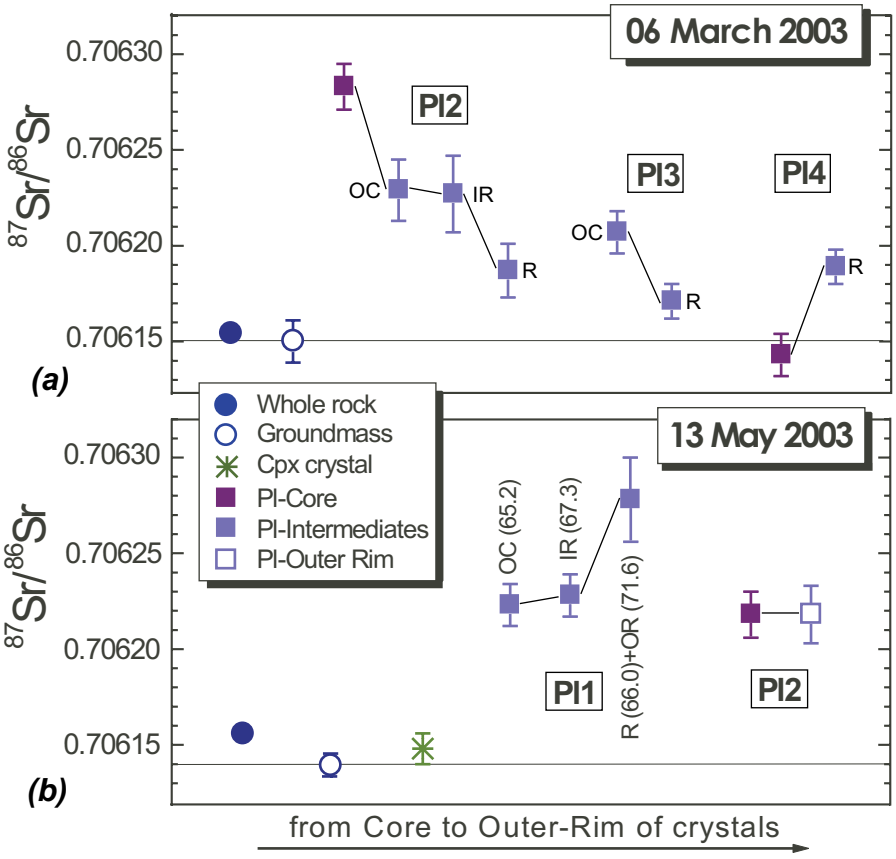
06 March 2003
0.70630
0.70625
0.70620
0.70615
87Sr/86Sr
(a)
PI2
OC
IR
R
PI3
OC
R
PI4
R
Whole rock
Groundmass
Cpx crystal
PI-Core
PI-Intermediates
PI-Outer Rim
13 May 2003
0.70630
0.70625
0.70620
0.70615
87Sr/86Sr
(b)
OC (65.2)
IR (67.3)
R (66.0)+OR (71.6)
PI1
PI2
from Core to Outer-Rim of crystals

Fig. 6

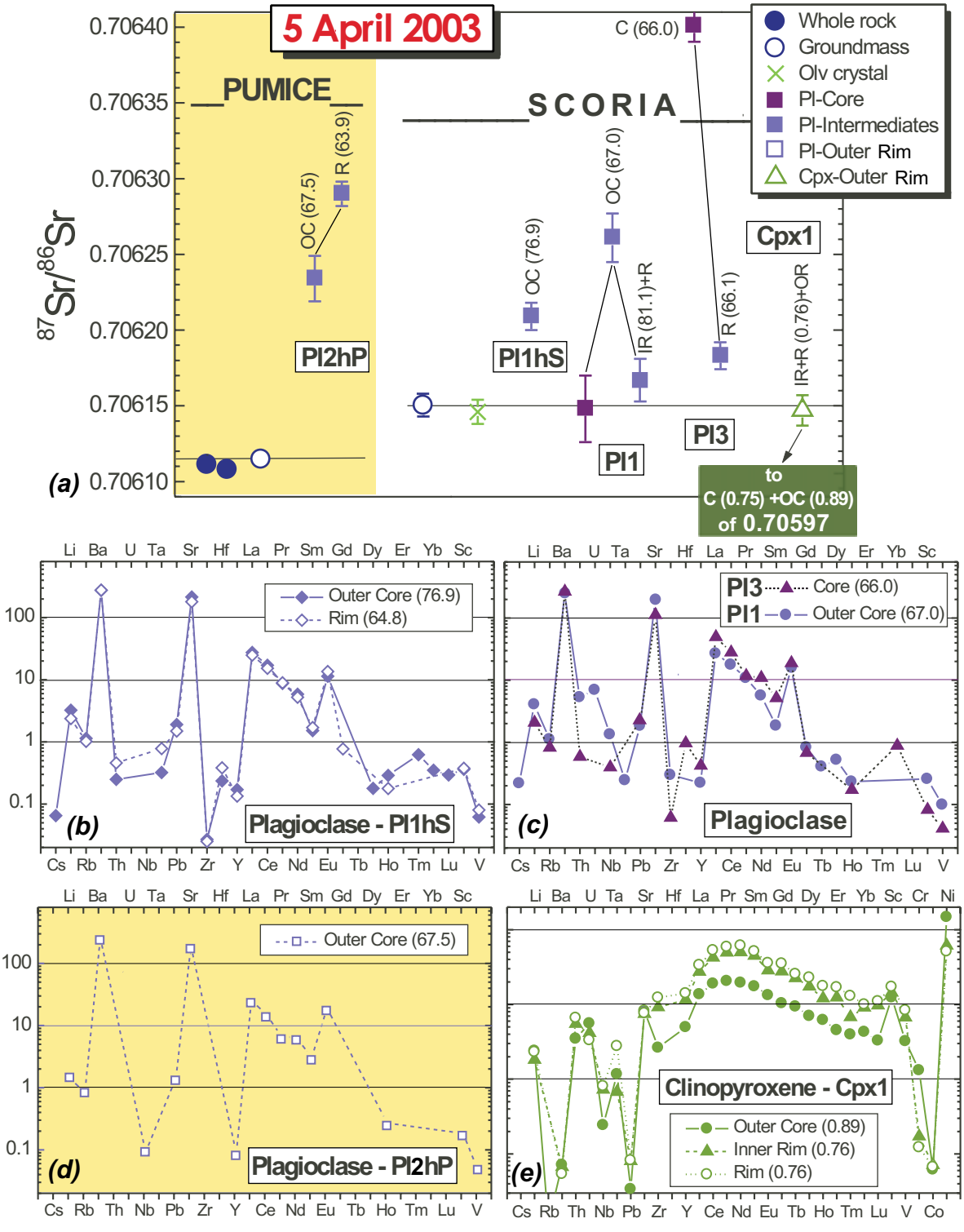
5 April 2003
PUMICE
SCORIA
Whole rock
Groundmass
Olv crystal
Pl-Core
Pl-Intermediates
Pl-Outer Rim
Cpx-Outer Rim
87Sr/86Sr
0.70640
0.70635
0.70630
0.70625
0.70620
0.70615
0.70610
(a)
OC (67.5)
R (63.9)
Pl2hP
OC (76.9)
Pl1hS
OC (67.0)
IR (81.1)+R
Pl1
C (66.0)
R (66.1)
Pl3
Cpx1
IR+R (0.76)+OR
to
C (0.75) +OC (0.89)
of 0.70597
Li Ba U Ta Sr Hf La Pr Sm Gd Dy Er Yb Sc
Cs Rb Th Nb Pb Zr Y Ce Nd Eu Tb Ho Tm Lu V
100
10
1
0.1
Outer Core (76.9)
Rim (64.8)
(b)
Plagioclase - Pl1hS
Pl3 Core (66.0)
Pl1 Outer Core (67.0)
(c)
Plagioclase
Outer Core (67.5)
(d)
Plagioclase - Pl2hP
Li Ba U Ta Sr Hf La Pr Sm Gd Dy Er Yb Sc Cr Ni
Cs Rb Th Nb Pb Zr Y Ce Nd Eu Tb Ho Tm Lu V Co
Clinopyroxene - Cpx1
Outer Core (0.89)
Inner Rim (0.76)
Rim (0.76)
(e)

Fig. 7

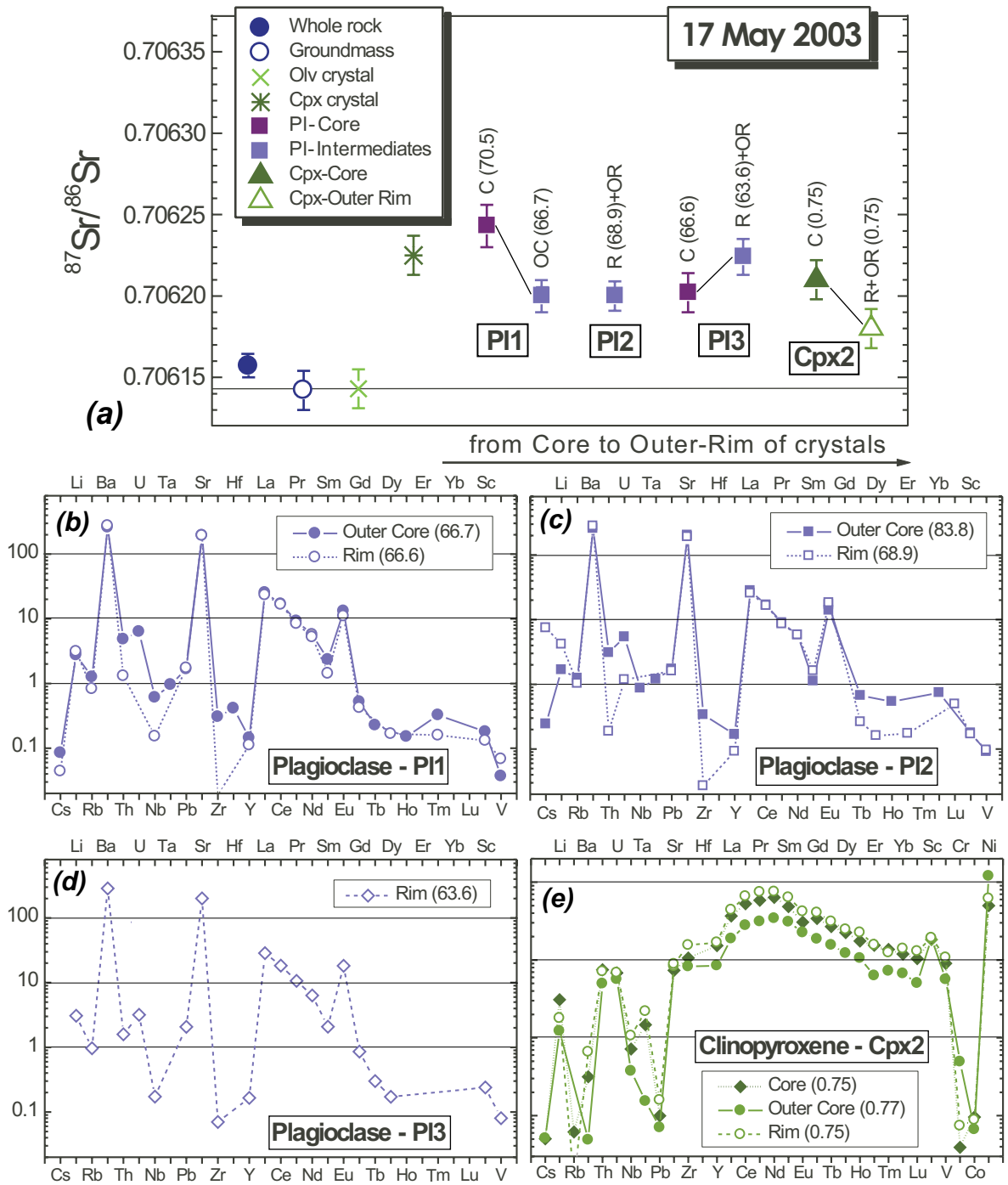
17 May 2003
Whole rock
Groundmass
Olv crystal
Cpx crystal
Pl-Core
Pl-Intermediates
Cpx-Core
Cpx-Outer Rim
87Sr/86Sr
0.70635
0.70630
0.70625
0.70620
0.70615
C (70.5)
OC (66.7)
R (68.9)+OR
C (66.6)
R (63.6)+OR
C (0.75)
R+OR (0.75)
Pl1
Pl2
Pl3
Cpx2
(a)
from Core to Outer-Rim of crystals
(b)
Outer Core (66.7)
Rim (66.6)
Plagioclase - Pl1
(c)
Outer Core (83.8)
Rim (68.9)
Plagioclase - Pl2
(d)
Rim (63.6)
Plagioclase - Pl3
(e)
Clinopyroxene - Cpx2
Core (0.75)
Outer Core (0.77)
Rim (0.75)
Li Ba U Ta Sr Hf La Pr Sm Gd Dy Er Yb Sc
Cs Rb Th Nb Pb Zr Y Ce Nd Eu Tb Ho Tm Lu V
Li Ba U Ta Sr Hf La Pr Sm Gd Dy Er Yb Sc Cr Ni
Cs Rb Th Nb Pb Zr Y Ce Nd Eu Tb Ho Tm Lu V Co
100
10
1
0.1

Fig. 8

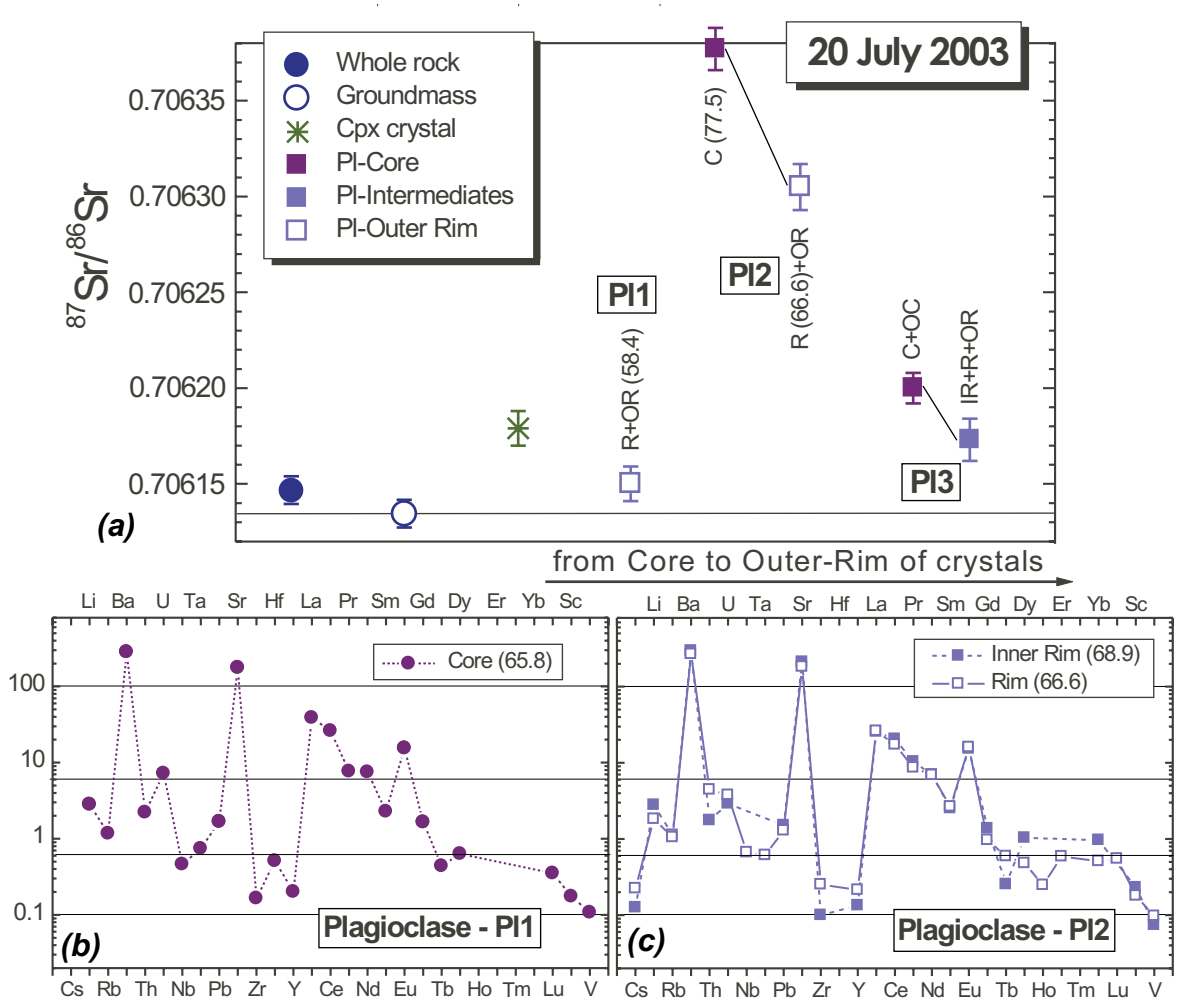
20 July 2003
Whole rock
Groundmass
Cpx crystal
Pl-Core
Pl-Intermediates
Pl-Outer Rim
$^{87}Sr/^{86}Sr$
0.70635
0.70630
0.70625
0.70620
0.70615
C (77.5)
R (66.6)+OR
R+OR (58.4)
C+OC
IR+R+OR
Pl1
Pl2
Pl3
(a)
from Core to Outer-Rim of crystals
Li Ba U Ta Sr Hf La Pr Sm Gd Dy Er Yb Sc
Core (65.8)
100
10
1
0.1
(b)
Plagioclase - Pl1
Inner Rim (68.9)
Rim (66.6)
(c)
Plagioclase - Pl2
Cs Rb Th Nb Pb Zr Y Ce Nd Eu Tb Ho Tm Lu V

Fig. 9

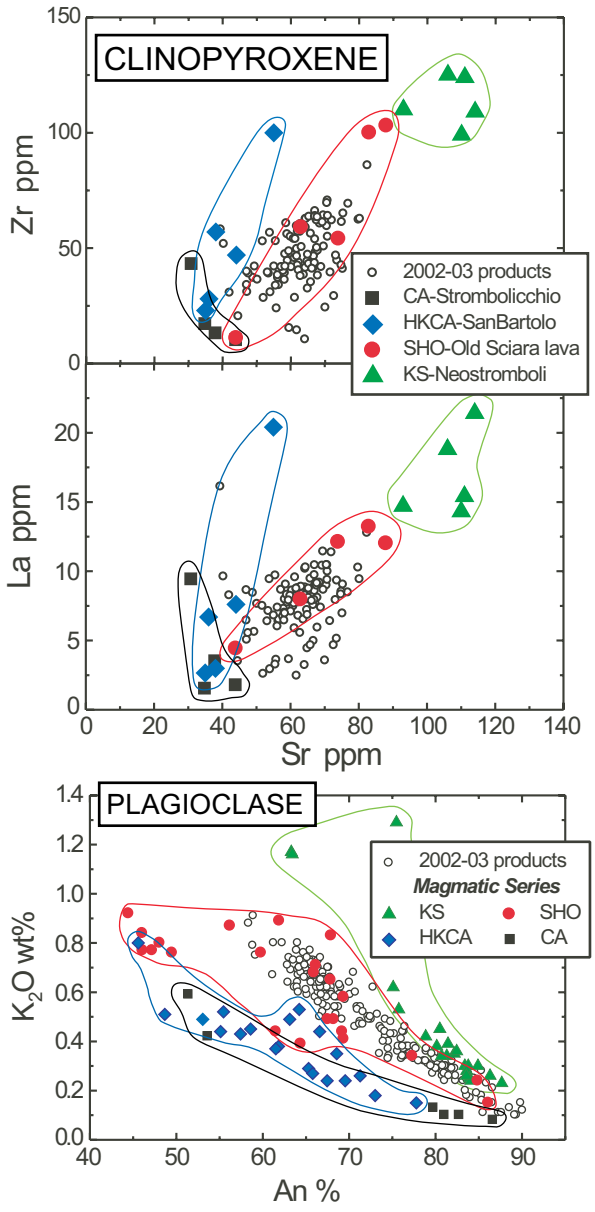
CLINOPYROXENE
Zr ppm
La ppm
Sr ppm
2002-03 products
CA-Strombolicchio
HKCA-SanBartolo
SHO-Old Sciara lava
KS-Neostromboli
PLAGIOCLASE
K2O wt%
An %
Magmatic Series
KS
SHO
HKCA
CA

Fig. 10

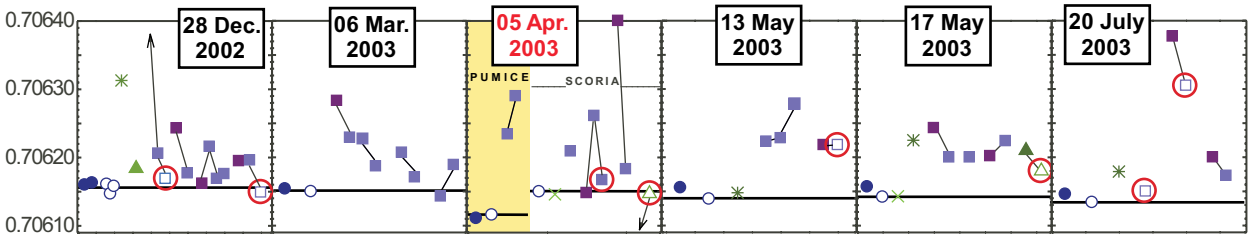
0.70640
0.70630
0.70620
0.70610
28 Dec. 2002
06 Mar. 2003
05 Apr. 2003
PUMICE
SCORIA
13 May 2003
17 May 2003
20 July 2003

Fig. 11

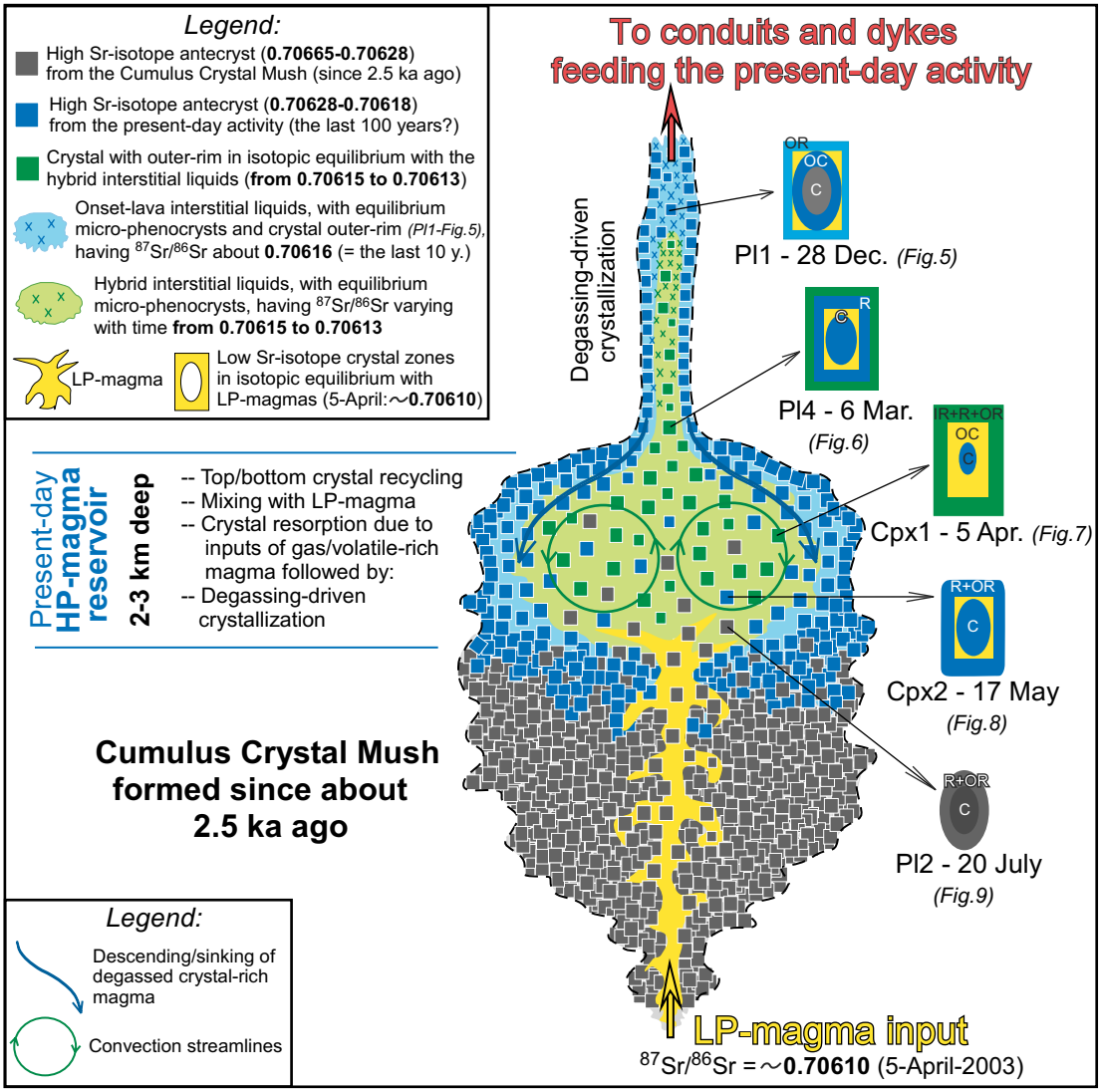
Legend:
High Sr-isotope antecryst (0.70665-0.70628) from the Cumulus Crystal Mush (since 2.5 ka ago)
High Sr-isotope antecryst (0.70628-0.70618) from the present-day activity (the last 100 years?)
Crystal with outer-rim in isotopic equilibrium with the hybrid interstitial liquids (from 0.70615 to 0.70613)
Onset-lava interstitial liquids, with equilibrium micro-phenocrysts and crystal outer-rim (Pl1-Fig.5), having 87Sr/86Sr about 0.70616 (= the last 10 y.)
Hybrid interstitial liquids, with equilibrium micro-phenocrysts, having 87Sr/86Sr varying with time from 0.70615 to 0.70613
LP-magma
Low Sr-isotope crystal zones in isotopic equilibrium with LP-magmas (5-April: ~0.70610)
To conduits and dykes feeding the present-day activity
Degassing-driven crystallization
OR
OC
C
Pl1 - 28 Dec. (Fig.5)
R
C
Pl4 - 6 Mar.
(Fig.6)
R+R+OR
OC
C
Cpx1 - 5 Apr. (Fig.7)
R+OR
C
Cpx2 - 17 May
(Fig.8)
R+OR
C
Pl2 - 20 July
(Fig.9)
Present-day HP-magma reservoir
2-3 km deep
-- Top/bottom crystal recycling
-- Mixing with LP-magma
-- Crystal resorption due to inputs of gas/volatile-rich magma followed by:
-- Degassing-driven crystallization
Cumulus Crystal Mush formed since about 2.5 ka ago
LP-magma input
87Sr/86Sr = ~0.70610 (5-April-2003)
Legend:
Descending/sinking of degassed crystal-rich magma
Convection streamlines

Fig. 12

Table 1 – Trace element contents and compositional end-members in the clinopyroxene crystals analysed for micro-Sr isotope ratios, from the 2002-2003 Stromboli products.

Date	28/12/2002	28/12/2002	28/12/2002	05/04/2003	05/04/2003	05/04/2003	17/05/2003	17/05/2003	17/05/2003
Lithotype	*Lava*	*Lava*	*Lava*	*Scoria*	*Scoria*	*Scoria*	*Lava*	*Lava*	*Lava*
Sample	**STR12/02a**	**STR12/02a**	**STR12/02a**	**STR050403f**	**STR050403f**	**STR050403f**	**STR170503**	**STR170503**	**STR170503**
Crystal	**Cpx13**	**Cpx13**	**Cpx13**	**Cpx1**	**Cpx1**	**Cpx1**	**Cpx2**	**Cpx2**	**Cpx2**
Zone	inner rim	rim	outer rim	outer core	inner rim	rim	core	outer core	rim
Li	-	1.37	2.22	3.60	2.73	3.47	4.64	1.84	2.69
B	-	-	-	1.42	-	-	3.03	2.65	-
Sc	98.1	102.5	126.1	72.1	83.9	100.1	106.2	110.3	112.0
Ti	4904	5679	6962	1526	3445	4650	4029	3516	5446
V	378	494	672	183	380	472	513	318	608
Cr	348	212	232	3506	457	328	104	1315	197
Co	27.4	35.2	42.8	31.0	35.6	33.5	48.2	33.5	44.3
Ni	0.00	0.00	0.00	162	67.4	56.1	55.0	132	67.6
Rb	-	0.04	0.03	0.03	-	-	0.14	-	0.03
Sr	42.1	60.9	67.2	64.2	58.2	59.6	57.3	65.0	69.4
Y	15.6	24.2	27.1	7.74	18.0	22.0	23.8	13.2	26.2
Zr	30.6	54.0	63.8	10.4	36.2	48.6	41.7	32.4	61.1
Nb	-	0.238	0.284	0.060	0.178	0.198	0.176	0.093	0.262
Cs	0.037	-	0.010	-	-	-	0.009	0.010	-
Ba	0.145	0.474	0.533	0.167	0.157	0.127	0.739	0.114	1.54
La	8.26	7.44	8.94	3.21	6.44	7.89	8.64	4.42	10.4
Ce	28.0	29.5	34.8	11.5	25.5	32.0	31.9	16.8	39.7
Pr	4.02	4.70	5.60	1.84	4.41	5.25	5.21	2.78	6.64
Nd	23.1	25.0	29.5	8.85	22.5	27.7	28.9	15.5	34.1
Sm	5.22	7.00	7.58	2.56	6.59	7.56	7.13	4.54	9.36
Eu	1.17	1.55	2.00	0.744	1.60	2.00	1.72	1.26	2.36
Gd	4.86	5.81	6.92	2.04	5.43	6.92	6.72	3.66	7.99
Tb	0.801	0.797	1.00	0.341	0.816	0.928	0.976	0.566	1.13
Dy	4.94	4.74	5.66	1.70	4.22	5.56	5.45	2.96	5.98
Ho	0.722	0.893	1.03	0.344	0.670	0.979	0.976	0.588	1.26
Er	1.69	2.33	2.80	0.720	1.96	2.70	2.45	1.00	2.49
Tm	0.315	0.311	0.329	0.096	0.164	0.314	0.331	0.175	0.302
Yb	2.74	2.17	2.41	0.697	1.47	1.62	1.94	1.09	2.28
Lu	0.332	0.243	0.289	0.080	0.235	0.268	0.253	0.123	0.315
Hf	1.00	2.09	2.47	0.45	1.57	2.03	1.55	1.47	2.13
Ta	-	0.047	0.032	0.016	0.010	0.039	0.021	0.002	0.031
Pb	0.627	0.270	0.339	0.084	0.199	0.203	0.246	0.174	0.391
Th	0.134	0.168	0.250	0.103	0.162	0.194	0.221	0.146	0.209
U	-	0.031	0.043	0.045	0.034	0.027	0.055	0.046	0.056
Eu/Eu*	0.69	0.72	0.82	0.96	0.79	0.83	0.74	0.91	0.81
La_N/Sm_N	0.99	0.67	0.74	0.79	0.61	0.65	0.76	0.61	0.70
Gd_N/Yb_N	1.47	2.22	2.37	2.41	3.05	3.53	2.86	2.78	2.90
En	42.8	nd	42.6	49.2	42.5	42.3	41.1	45.2	41.0
Fe	15.7	nd	14.3	5.9	13.6	13.7	13.7	13.6	13.7
Wo	41.5	nd	43.1	44.8	43.9	44.0	45.2	41.2	45.2
Mg#	0.73	nd	0.75	0.89	0.76	0.76	0.75	0.77	0.75

En: Enstatite, Fs: Ferrosilite, Wo: Wollastonite, Mg# [molar $Mg/(Mg+Fe^{2+})$]: Mg-value; "-": below detection limits;
nd: not determined; N: Chondrite-normalised (Anders and Grevesse, 1989).

Table 2a – Trace element contents and compositional end-members in the plagioclase crystals analysed for micro-Sr isotope ratios, from the 2002-2003 Stromboli products.

Date	28/12/2002	28/12/2002	28/12/2002	28/12/2002	05/04/2003	05/04/2003	05/04/2003	05/04/2003	05/04/2003
Lithotype	*Lava*	*Lava*	*Lava*	*Lava*	*Scoria*	*Scoria*	*Scoria*	*Scoria*	*Pumice*
Sample	**STR12/02a**	**STR12/02a**	**STR12/02a**	**STR12/02a**	**STR050403f**	**STR050403f**	**STR050403hS**	**STR050403hS**	**STR050403hP**
Crystal	**Pl2**	**Pl2**	**Pl4**	**Pl4**	**Pl1**	**Pl3**	**Pl1hS**	**Pl1hS**	**Pl2hP**
Zone	***inner rim***	***outer rim***	***inner rim***	***outer rim***	***outer core***	***core***	***outer core***	***rim***	***outer core***
Li	4.39	5.81	6.39	4.27	5.21	3.11	4.84	3.56	2.40
B	-	-	-	-	-	-	2.42	-	-
Sc	1.83	1.31	1.11	1.16	1.51	0.479	2.11	2.19	1.08
Ti	602	477	482	505	380	253	365	362	356
V	4.93	3.47	3.63	4.24	6	2.33	3.53	4.54	2.64
Cr	0.221	-	2.37	-	-	0.948	-	3.46	-
Co	0.961	0.890	0.603	0.870	1.07	0.366	0.960	0.570	1.12
Ni	-	-	-	-	0.26	0.211	0.424	0.323	0.636
Rb	3.18	2.62	1.95	2.31	2.6	1.89	2.62	2.34	2.10
Sr	1993	1668	1668	1495	1551	877	1677	1402	1474
Y	0.263	0.237	0.302	0.236	0.35	0.657	0.267	0.210	0.139
Zr	0.171	0.619	0.130	0.293	1.2	0.24	0.11	0.10	-
Nb	0.051	0.042	0.025	0.041	0.3	0.098	-	-	0.02
Cs	0.008	-	-	-	0.04	-	0.01	-	-
Ba	767	701	722	631	590	621	644	648	607
La	6.74	5.97	7.26	5.43	6.3	11.6	6.47	5.83	5.97
Ce	11.0	9.92	11.4	8.59	10.8	16.9	10.3	9.22	9.05
Pr	0.920	0.727	0.938	0.699	0.97	1.04	0.781	0.797	0.589
Nd	3.17	2.22	3.02	2.61	2.6	4.92	2.64	2.36	2.89
Sm	0.296	0.314	0.424	0.172	0.28	0.756	0.223	0.251	0.449
Eu	0.990	0.738	0.823	0.749	0.89	1.05	0.639	0.759	1.07
Gd	0.109	0.114	0.278	0.115	0.16	0.133	-	0.152	-
Tb	0.014	0.014	0.007	0.013	0.015	-	-	-	-
Dy	0.040	0.043	0.108	0.085	0.13	-	0.044	-	-
Ho	0.010	0.007	0.002	0.006	0.013	0.010	0.016	0.010	0.015
Er	0.027	0.019	0.004	0.012	-	-	-	-	-
Tm	0.001	0.001	0.003	-	-	-	0.015	-	-
Yb	0.021	-	-	0.007	-	0.144	0.057	-	-
Lu	0.002	0.002	-	0.005	-	-	0.007	-	-
Hf	-	-	-	0.013	-	0.100	0.025	0.040	-
Ta	0.004	0.005	0.002	-	0.003	-	0.005	0.011	-
Pb	6.67	5.34	5.56	4.86	4.61	5.60	4.71	3.68	3.55
Th	0.011	0.019	0.016	0.015	0.157	0.017	0.007	0.013	-
U	-	0.01	-	-	0.06	-	-	-	-
Eu/Eu*	13.8	9.70	6.85	15.2	11.8	6.46	-	11.0	-
La_N/Sm_N	14.3	11.9	10.7	19.8	14.4	9.61	18.2	14.6	8.33
Gd_N/Yb_N	4.29			13.62	-	0.77			
An	71.0	68.6	65.8	64.7	67.0	66.0	76.9	64.8	67.5
Ab	25.6	27.9	29.6	30.6	28.9	30.3	20.7	30.8	28.6
Or	3.1	3.3	4.3	4.4	4.0	3.8	2.2	3.8	3.8
Cs	0.3	0.1	0.32	0.25	0.14	-	0.22	0.54	0.11

"-": below detection limits; nd: not determined. An: Anorthite, Ab: Albite, Or: Orthoclase, Cn: Celsian;
N: Chondrite-normalised (Anders and Grevesse, 1989).

Table 2b – Trace element contents and compositional end-members in the plagioclase crystals analysed for micro-Sr isotope ratios, from the 2002-2003 Stromboli products

Date	17/05/2003	17/05/2003	17/05/2003	17/05/2003	17/05/2003	20/07/2003	20/07/2003	20/07/2003
Lithotype	*Lava*	*Lava*	*Lava*	*Lava*	*Lava*	*Lava*	*Lava*	*Lava*
Sample	**STR170503**	**STR170503**	**STR170503**	**STR170503**	**STR170503**	**STR200703**	**STR200703**	**STR200703**
Crystal	**Pl1**	**Pl1**	**Pl2**	**Pl2**	**Pl3**	**Pl1**	**Pl2**	**Pl2**
Zone	***outer core***	***rim***	***outer core***	***rim***	***rim***	***core***	***rim***	***inner rim***
Li	4.11	4.69	3.47	4.06	3.59	4.24	2.74	4.19
B	2.58	-	-	1.87	3.28	2.23	-	-
Sc	1.05	0.76	1.03	0.99	1.40	1.02	1.05	1.34
Ti	342	325	387	383	351	437	400	373
V	2.08	3.86	5.12	5.4	4.5	6.07	5.47	4.22
Cr	-	-	1.67	-	-	-	-	-
Co	1.76	0.836	0.80	1.89	0.85	0.943	0.791	0.854
Ni	0.645	0.496	0.84	-	0.46	0.445	0.333	0.607
Rb	2.90	1.91	2.86	2.4	2.22	2.70	2.42	2.60
Sr	1520	1510	1509	1485	1561	1386	1420	1649
Y	0.224	0.175	0.262	0.14	0.26	0.314	0.333	0.209
Zr	1.21	0.07	1.33	0.1	0.28	0.65	0.99	0.39
Nb	0.15	0.04	0.21	-	0.04	0.11	0.16	-
Cs	0.02	0.01	0.05	1.40	-	-	0.04	0.02
Ba	609	642	603	655	671	662	627	694
La	5.96	5.47	6.55	6.0	6.72	9.10	6.15	5.99
Ce	10.2	10.0	10.15	9.9	11.0	15.8	10.4	12.4
Pr	0.823	0.753	0.797	0.76	0.95	0.683	0.772	0.922
Nd	2.59	2.37	2.62	2.6	2.87	3.39	3.13	3.15
Sm	0.346	0.211	0.165	0.24	0.307	0.336	0.391	0.371
Eu	0.739	0.615	0.778	1.02	1.021	0.867	0.896	0.854
Gd	0.103	0.083	-	-	0.169	0.325	0.191	0.270
Tb	0.008	-	0.024	0.010	0.011	0.016	0.021	0.009
Dy	-	0.040	-	0.04	0.042	0.154	0.116	0.251
Ho	0.008	-	0.030	-	-	-	0.01	-
Er	-	-	-	0.028	-	-	0.09	-
Tm	0.008	0.004	-	-	-	-	-	-
Yb	-	-	0.121	-	-	-	0.08	0.16
Lu	-	-	-	0.012	-	0.01	0.01	-
Hf	0.043	-	-	-	-	0.05	-	-
Ta	0.014	-	0.017	-	-	0.011	0.009	-
Pb	4.12	4.29	4.25	3.96	5.13	4.14	3.18	3.72
Th	0.142	0.039	0.090	0.006	0.047	0.065	0.131	0.052
U	0.051	-	0.044	0.01	0.026	0.059	0.030	0.024
Eu/Eu*	9.18	11.8	-	-	12.4	7.86	7.84	8.82
La_N/Sm_N	10.8	16.2	24.8	15.8	13.7	17.0	10.1	9.86
Gd_N/Yb_N	-	-	-	-	-	-	1.42	1.90
An	66.7	66.6	83.8	68.9	63.6	65.8	66.6	68.9
Ab	29.4	29.3	14.4	27.4	31.8	29.9	29.4	27.2
Or	3.6	3.8	1.6	3.5	4.3	4.0	3.7	3.8
Cs	0.29	0.26	0.18	0.22	0.29	0.22	0.25	0.18

"-": below detection limits; nd: not determined. An: Anorthite, Ab: Albite, Or: Orthoclase, Cn: Celsian;
N: Chondrite-normalised (Anders and Grevesse, 1989).

Table 3a - Sr isotope ratios in whole-rocks, groundmasses and minerals (micro-drilled and separated) from the 2002-03 Stromboli prod

DATE	PRODUCT	SAMPLE	TYPE	CRYSTAL ZONE & DETAILS	L(mm)	DEPTH	TRACE	$^{87}Sr/^{86}Sr$	$2\sigma*10^6$
28 Dec. 2002	Lava	STR12/02a	**Whole rock**	-	**-**	**(μm)**	**-**	***0.706160****	**5**
28 Dec. 2002	Lava	STR12/02a	**Groundmass**	drilled	-	50	-	**0.706161**	**12**
28 Dec. 2002	Lava	STR12/02a	**Groundmass**	drilled	-	50	-	**0.706147**	**14**
28 Dec. 2002	Lava	STR12/02a	**Plagioclase-Pl1**	C	1.5	50	-	**0.706647**	**11**
28 Dec. 2002	Lava	STR12/02a	**Plagioclase-Pl1**	OC	1.5	50	-	**0.706206**	**9**
28 Dec. 2002	Lava	STR12/02a	**Plagioclase-Pl1**	OR	1.5	50	-	**0.706169**	**11**
28 Dec. 2002	Lava	STR12/02a	**Plagioclase-Pl2**	C(83.4)	1.5	50	-	**0.706243**	**11**
28 Dec. 2002	Lava	STR12/02a	**Plagioclase-Pl2**	IR(71.0)+R(80.0)+OR(68.6)	1.5	50	IR, OR	**0.706177**	**10**
28 Dec. 2002	Lava	STR12/02a	**Plagioclase-Pl3**	C	1.3	50	-	**0.706162**	**10**
28 Dec. 2002	Lava	STR12/02a	**Plagioclase-Pl3**	OR	1.3	50	-	**0.706216**	**12**
28 Dec. 2002	Lava	STR12/02a	**Plagioclase-Pl3**	IR	1.3	50	-	**0.706169**	**11**
28 Dec. 2002	Lava	STR12/02a	**Plagioclase-Pl3**	R	1.3	50	-	**0.706176**	**11**
28 Dec. 2002	Lava	STR12/02a	**Plagioclase-Pl4**	C(80.6)	1.2	50	-	**0.706195**	**16**
28 Dec. 2002	Lava	STR12/02a	**Plagioclase-Pl4**	OC(72.3)+IR(65.8)	1.2	50	IR	**0.706196**	**11**
28 Dec. 2002	Lava	STR12/02a	**Plagioclase-Pl4**	R(81.9)+OR(64.7)	1.2	60	OR	**0.706149**	**11**
28 Dec. 2002	Lava	STR12/02a	**Clinopyroxene**	separated single crystal	-	-	-	**0.706313**	**7**
28 Dec. 2002	Lava	STR12/02a	**Clinopyroxene-Cpx13**	IR(0.73)+R+OR(0.75)	4.5	50	IR,R,OR	**0.706184**	**10**
28 Dec. 2002	Lava	STR12/02b	**Whole rock**	-	-	-	-	***0.706163****	**4**
28 Dec. 2002	Lava	STR12/02b	**Groundmass**	separated	-	-	-	**0.706158**	**4**
15 Jan. 2003	Lava	STR150103	**Whole rock**	-	-	-	-	***0.706163****	**5**
15 Jan. 2003	Lava	STR150103	**Groundmass**	separated	-	-	-	**0.706156**	**5**
1 Feb. 2003	Lava	STR010203	**Whole rock**	-	-	-	-	***0.706152****	**6**
17 Feb. 2003	Lava	STR170203	**Whole rock**	-	-	-	-	***0.706160****	**7**
17 Feb. 2003	Lava	STR170203	**Groundmass**	separated	-	-	-	**0.706149**	**8**
4 March 2003	Lava	STR040303	**Whole rock**	-	-	-	-	***0.706154****	**6**
6 March 2003	Lava	STR060303	**Groundmass**	drilled	-	70	-	**0.706150**	**11**
6 March 2003	Lava	STR060303	**Plagioclase-Pl2**	C	1.6	60	-	**0.706283**	**12**
6 March 2003	Lava	STR060303	**Plagioclase-Pl2**	OR	1.6	60	-	**0.706229**	**16**
6 March 2003	Lava	STR060303	**Plagioclase-Pl2**	IR	1.6	60	-	**0.706227**	**20**
6 March 2003	Lava	STR060303	**Plagioclase-Pl2**	R	1.6	60	-	**0.706187**	**14**
6 March 2003	Lava	STR060303	**Plagioclase-Pl3**	OC	1.2	60	-	**0.706207**	**11**
6 March 2003	Lava	STR060303	**Plagioclase-Pl3**	R	1.2	60	-	**0.706171**	**9**
6 March 2003	Lava	STR060303	**Plagioclase-Pl4**	C	2.5	60	-	**0.706143**	**11**
6 March 2003	Lava	STR060303	**Plagioclase-Pl4**	R	2.5	60	-	**0.706189**	**9**
18 March 2003	Lava	STR180303	**Groundmass**	separated	-	-	-	**0.706151**	**7**
5 April 2003	Scoria	STR050403hi	**Groundmass**	separated	-	-	-	**0.706150**	**7**
5 April 2003	Scoria	STR050403hS	**Plagioclase-Pl1hS**	OC(76.9)	1.0	60	OC,R	**0.706209**	**9**
5 April 2003	Scoria	STR050403hS	**Olivine**	separated single crystal	-	-	-	**0.706146**	**8**
5 April 2003	Scoria	STR050403f	**Plagioclase-Pl1**	C	1.5	60		**0.706148**	**22**
5 April 2003	Scoria	STR050403f	**Plagioclase-Pl1**	OC(67.0)	1.5	60	OC	**0.706261**	**16**
5 April 2003	Scoria	STR050403f	**Plagioclase-Pl1**	IR(81.1)+R	1.5	60	IR	**0.706167**	**14**
5 April 2003	Scoria	STR050403f	**Plagioclase-Pl3**	C(66.0)	0.7	70	C	**0.706401**	**11**
5 April 2003	Scoria	STR050403f	**Plagioclase-Pl3**	R(66.1)	0.7	70	R	**0.706183**	**9**
5 April 2003	Scoria	STR050403f	**Clinopyroxene-Cpx1**	C(0.75)+OC(0.89)	2.5	70	OC	**0.705966**	**12**
5 April 2003	Scoria	STR050403f	**Clinopyroxene-Cpx1**	IR+R(0.76)+OR	2.5	70	IR,R	**0.706147**	**10**
5 April 2003	Pumice	STR050403k	**Whole rock**	-	-	-	-	**0.706098**	**7**
5 April 2003	Pumice	STR050403hP	**Whole rock**	-	-	-	-	**0.706111**	**7**
5 April 2003	Pumice	STR050403hP	**Groundmass**	separated	-	-	-	**0.706116**	**5**
5 April 2003	Pumice	STR050403hP	**Plagioclase-Pl2hP**	OC(67.5)	1.5	60	C,OC	**0.706234**	**15**
5 April 2003	Pumice	STR050403hP	**Plagioclase-Pl2hP**	R(63.9)	1.5	60	-	**0.706290**	**8**

L: lenght of crystal, DEPTH: depth of drilling, TRACE: zones analysed for trace elements. Asterisks & italics: data from Landi et al., (2006).
C: core, OC: outer core, IR: inner rim, R: rim, OR: outer rim; numbers in brackets indicate anorthite content and Mg# [molar $Mg/(Mg+Fe^{2+})$] for plagioclase and clinopyroxene, respectively. "-": no significant or available data. All the data from microdrilling are those with reported DEPTH.

Table 3b - Sr isotope ratios in whole-rocks, groundmasses and minerals (micro-drilled and separated) from the 2002-03 Stromboli proc

DATE	PRODUCT	SAMPLE	TYPE	CRYSTAL ZONE & DETAILS	L(mm)	DEPTH	TRACE	$^{87}Sr/^{86}Sr$	$2\sigma*10^6$
14 April 2003	Lava	STR140403	**Whole rock**	-	-	-	-	***0.706156****	**8**
14 April 2003	Lava	STR140403	**Groundmass**	-	-	-	-	**0.706151**	**7**
14 April 2003	Lava	STR140403	**Plagioclase**	separated single crystal	-	-	-	**0.706183**	**6**
14 April 2003	Lava	STR140403	**Olivine**	separated single crystal	-	-	-	**0.706193**	**8**
13 May 2003	Lava	STR130503	**Whole rock**	-	-	-	-	***0.706156****	**6**
13 May 2003	Lava	STR130503	**Groundmass**	separated	-	-	-	**0.706139**	**6**
13 May 2003	Lava	STR130503	**Plagioclase-Pl1**	OC(65.2)	2.1	60	-	**0.706223**	**11**
13 May 2003	Lava	STR130503	**Plagioclase-Pl1**	IR(67.3)	2.1	60	-	**0.706228**	**11**
13 May 2003	Lava	STR130503	**Plagioclase-Pl1**	R(66.0)-OR(71.6)	2.1	60	-	**0.706278**	**22**
13 May 2003	Lava	STR130503	**Plagioclase-Pl2**	C	1.3	60	-	**0.706218**	**12**
13 May 2003	Lava	STR130503	**Plagioclase-Pl2**	OR	1.3	60	-	**0.706218**	**15**
13 May 2003	Lava	STR130503	**Clinopyroxene**	separated single crystal	-	-	-	**0.706148**	**8**
17 May 2003	Lava	STR170503	**Whole rock**	-	-	-	-	**0.706157**	**7**
17 May 2003	Lava	STR170503	**Groundmass**	drilled	-	70	-	**0.706142**	**12**
17 May 2003	Lava	STR170503	**Plagioclase-Pl1**	C(70.5)	1.5	60	C	**0.706243**	**13**
17 May 2003	Lava	STR170503	**Plagioclase-Pl1**	OC(66.7)	1.5	60	OC,R	**0.706200**	**10**
17 May 2003	Lava	STR170503	**Plagioclase-Pl2**	R(68.9)+OR	2.0	60	C,OC,R	**0.706200**	**9**
17 May 2003	Lava	STR170503	**Plagioclase-Pl3**	C(66.6)	1.5	60	OC	**0.706202**	**12**
17 May 2003	Lava	STR170503	**Plagioclase-Pl3**	R(63.6)	1.5	60	R	**0.706224**	**11**
17 May 2003	Lava	STR170503	**Clinopyroxene**	separated single crystal	1.5	-	-	**0.706225**	**12**
17 May 2003	Lava	STR170503	**Olivine**	separated single crystal	1.2	-	-	**0.706143**	**12**
17 May 2003	Lava	STR170503	**Clinopyroxene-Cpx2**	C(0.75)	2.0	70	C,OC	**0.706210**	**12**
17 May 2003	Lava	STR170503	**Clinopyroxene-Cpx2**	R+OR(0.75)	2.0	70	R	**0.706180**	**12**
6 June 2003	Lava	STR060603	**Whole rock**	-	-	-	-	***0.706149****	**7**
3 July 2003	Lava	STR030703	**Whole rock**	-	-	-	-	***0.706150****	**8**
3 July 2003	Lava	STR030703	**Groundmass**	separated	-	-	-	**0.706141**	**6**
20 July 2003	Lava	STR200703	**Whole rock**	-	-	-	-	***0.706146****	**7**
20 July 2003	Lava	STR200703	**Groundmass**	separated	-	-	-	**0.706134**	**7**
20 July 2003	Lava	STR200703	**Plagioclase-Pl1**	R+OR(58.4)	0.7	50	C,R	**0.706150**	**9**
20 July 2003	Lava	STR200703	**Plagioclase-Pl2**	C(77.5)	0.8	50	-	**0.706377**	**11**
20 July 2003	Lava	STR200703	**Plagioclase-Pl2**	R(66.6)+OR	0.8	50	IR,R	**0.706305**	**12**
20 July 2003	Lava	STR200703	**Plagioclase-Pl3**	C+OC	1.5	60	-	**0.706200**	**8**
20 July 2003	Lava	STR200703	**Plagioclase-Pl3**	IR+R+OR	1.5	50	-	**0.706173**	**11**
20 July 2003	Lava	STR200703	**Clinopyroxene**	separated single crystal	-	-	-	**0.706179**	**9**

L: lenght of crystal, DEPTH: depth of drilling, TRACE: zones analysed for trace elements. Asterisks & italics: data from Landi et al., (2006).
C: core, OC: outer core, IR: inner rim, R: rim, OR: outer rim; numbers in brackets indicate anorthite content and Mg# [molar $Mg/(Mg+Fe^{2+})$] for plagioclase and clinopyroxene, respectively. "-": no significant or available data. All the data from microdrilling are those with reported DEPTH.

Table ESM-1 - Electron microprobe analyses of the clinopyroxene micro-milled for Sr isotope data

Crystal	Cpx13	Cpx13	Cpx13	Cpx13	Cpx13	Cpx1	Cpx1	Cpx1	Cpx2	Cpx2	Cpx2
Type	*Lava*	*Lava*	*Lava*	*Lava*	*Lava*	*Scoria*	*Scoria*	*Scoria*	*Lava*	*Lava*	*Lava*
Sample	STR	STR	STR	STR	STR	STR	STR	STR	STR	STR	STR
Sample	12 02a	12 02a	12 02a	12 02a	12 02a	050403f	050403f	050403f	170503	170503	170503
Zone	core	core	outer-core	inner-rim	outer-rim	core	outer-core	rim	core	outer-core	outer-rim
SiO_2	52.29	53.17	54.73	51.63	51.38	51.81	53.28	51.63	50.24	52.42	49.48
TiO_2	0.84	0.37	0.17	0.78	0.79	0.74	0.20	0.70	0.93	0.61	1.00
Al_2O_3	3.08	2.92	1.64	3.65	2.93	2.64	1.98	2.89	3.88	1.64	4.14
Cr_2O3	bdl	0.60	0.84	0.21	0.04	0.06	0.57	0.15	0.02	0.22	0.10
Fe_2O_3	0.02			0.64	1.43	2.16	1.54	2.38	2.47	1.45	2.83
FeO	8.52	4.43	3.17	8.83	7.39	6.60	2.35	6.23	5.94	7.03	5.66
MnO	0.26	0.14	0.12	0.25	0.22	0.27	0.07	0.19	0.24	0.26	0.23
MgO	14.68	16.75	18.35	14.74	14.87	14.95	17.76	14.95	14.15	16.01	14.15
CaO	20.88	21.03	21.77	19.87	20.90	21.59	22.50	21.49	21.62	20.30	21.69
Na_2O	0.34	0.23	0.16	0.35	0.27	0.31	0.20	0.38	0.39	0.30	0.25
sum	100.91	99.64	100.97	100.95	100.22	101.13	100.46	100.99	99.88	100.23	99.53
En	42.4	48.7	51.2	42.8	42.6	42.2	49.2	42.5	41.1	45.2	41.0
Fe	14.3	7.4	5.2	15.7	14.3	14.0	5.9	13.6	13.7	13.6	13.7
Wo	43.3	43.9	43.7	41.5	43.1	43.8	44.8	43.9	45.2	41.2	45.2
Mg#	0.75	0.87	0.91	0.73	0.75	0.75	0.89	0.76	0.75	0.77	0.75

Mg# [molar $Mg^{2+}/(Mg^{2+}+Fe^{2+})$]: Mg-value; En: Enstatite, Fs: Ferrosilite, Wo: Wollastonite;
bdl: below detection limit (0.01 wt%, Vaggelli et al., 1999)

Table ESM-2 - Electron microprobe analyses of the plagioclase micro-milled for Sr isotope data

Crystal	Pl2	Pl2	Pl2	Pl2	Pl2	Pl4	Pl4	Pl4	Pl4	Pl4	Pl1	Pl1	Pl3	Pl3	Pl1hS	Pl1hS	Pl2hP	Pl2hP	Pl2hP
Type	*Lava*	*Lava*	*Lava*	*Lava*	*Lava*	*Lava*	*Lava*	*Lava*	*Lava*	*Lava*	*Scoria*	*Scoria*	*Scoria*	*Scoria*	*Scoria*	*Scoria*	*Pumice*	*Pumice*	*Pumice*
Sample	STR	STR	STR	STR	STR	STR	STR	STR	STR	STR	STR	STR	STR	STR	STR	STR	STR	STR	STR
Sample	1202a	1202a	1202a	1202a	1202a	1202a	1202a	1202a	1202a	1202a	050403f	050403f	050403f	050403f	050403hS	050403hS	050403hP	050403hP	050403hP
Zones	core	outer core	inner rim	rim	outer rim	core	outer core	inner rim	rim	outer rim	outer core	inner rim	core	rim	outer core	rim	core	outer core	rim
SiO_2	47.75	47.62	50.84	48.39	51.30	48.54	50.18	51.70	47.68	52.13	51.53	48.19	51.83	52.38	48.84	*51.92*	*49.50*	51.76	51.74
Al_2O_3	33.31	33.11	31.25	32.60	30.64	32.12	31.17	29.59	32.43	29.79	30.65	32.68	30.66	30.19	32.50	*30.34*	*31.38*	30.14	29.80
Fe_2O_3	0.90	0.80	0.82	0.90	0.99	1.00	0.80	1.09	1.00	0.95	1.08	1.12	1.00	0.95	1.00	*1.12*	*1.13*	1.12	1.08
MnO	0.04	0.04	bdl	0.01	bdl	bdl	bdl	bdl	0.02	bdl	0.13	0.04	0.14	0.15	0.15	*0.08*	*0.06*	0.10	0.08
CaO	16.88	16.88	14.43	16.25	14.14	16.33	15.00	13.41	16.54	13.31	13.52	16.20	13.40	13.29	15.62	*13.29*	*15.14*	13.09	12.89
Na_2O	1.68	1.66	2.88	2.00	3.18	1.96	2.83	3.33	1.80	3.48	3.22	1.88	3.40	3.29	2.32	*3.49*	*2.54*	3.07	3.50
K_2O	0.24	0.25	0.53	0.35	0.58	0.33	0.49	0.73	0.29	0.76	0.68	0.30	0.64	0.65	0.38	*0.66*	*0.40*	0.62	0.77
SrO	0.10	0.29	0.19	0.12	0.15	0.12	0.20	0.13	0.17	0.47	0.11	0.22	0.02	0.28	0.15	*0.09*	*0.13*	0.16	0.24
BaO	0.11	0.03	0.08	0.05	0.04	bdl	0.06	0.09	0.08	0.07	0.04	0.03	bdl	0.14	0.06	*0.15*	*0.12*	0.03	0.03
SUM	101.01	100.68	101.02	100.67	101.02	100.40	100.73	100.07	100.01	100.96	100.96	100.66	101.09	101.32	101.02	101.14	100.40	100.09	100.13
An	**83.2**	**83.5**	**71.0**	**80.0**	**68.6**	**80.6**	**72.3**	**65.8**	**81.9**	**64.7**	**67.0**	**81.1**	**66.0**	**66.1**	**76.9**	**64.8**	**74.6**	**67.5**	**63.9**
Ab	15.0	14.9	25.6	17.8	27.9	17.5	24.7	29.6	16.1	30.6	28.9	17.0	30.3	29.6	20.7	30.8	22.6	28.6	31.4
Or	1.4	1.5	3.1	2.1	3.3	1.9	2.8	4.3	1.7	4.4	4.0	1.8	3.8	3.8	2.2	3.8	2.3	3.8	4.5
Cs	0.4	0.1	0.3	0.2	0.1		0.2	0.3	0.3	0.2	0.1	0.1		0.5	0.2	0.5	0.4	0.1	0.1

Numbers in italics: not drilled zone for Sr isotopes; An: anorthite, Ab: albite, Or: orthoclase, Cn: Celsian; bdl: below detection limits (0.01 wt%, Vaggelli et al., 1999)

Crystal	Pl1	Pl1	Pl1	Pl1	Pl1	Pl1	Pl1	Pl1	Pl2	Pl2	Pl2	Pl3	Pl3	Pl3	Pl1	Pl1	Pl2	Pl2	Pl2
Type	*Lava*	*Lava*	*Lava*	*Lava*	*Lava*	*Lava*	*Lava*	*Lava*	*Lava*	*Lava*	*Lava*	*Lava*	*Lava*	*Lava*	*Lava*	*Lava*	*Lava*	*Lava*	*Lava*
Sample	STR	STR	STR	STR	STR	STR	STR	STR	STR	STR	STR	STR	STR	STR	STR	STR	STR	STR	STR
Sample	130503	130503	130503	130503	130503	170503	170503	170503	170503	170503	170503	170503	170503	170503	200703	200703	200703	200703	200703
Zones	core	outer core	inner rim	rim	outer rim	core	outer core	rim	core	outer core	rim	core	outer core	rim	core	outer rim	core	inner rim	rim
SiO_2	*48.23*	51.75	51.93	51.90	50.42	50.93	51.46	*51.42*	*49.32*	*47.42*	50.74	52.26	*52.01*	51.89	*52.17*	53.52	49.20	*51.11*	51.36
Al_2O_3	*32.59*	30.03	30.66	30.71	31.41	30.34	30.38	*30.04*	*32.11*	*33.60*	30.75	30.01	*30.01*	29.96	*30.45*	29.08	32.54	*31.14*	30.80
Fe_2O_3	*1.20*	1.23	0.98	0.95	1.02	1.61	1.23	*1.20*	*1.08*	*0.96*	0.86	1.21	*1.24*	1.12	*1.00*	0.98	1.03	*1.06*	0.97
MnO	*0.09*	0.16	0.13	0.12	0.13	0.11	0.13	*0.14*	*0.08*	*0.14*	0.15	0.10	*0.13*	0.09	*0.11*	0.09	0.08	*0.13*	0.12
CaO	*15.72*	12.95	13.35	13.29	14.54	14.17	13.61	*13.33*	*15.06*	*16.93*	13.88	13.41	*13.09*	12.86	*13.03*	11.85	15.61	*13.77*	13.59
Na_2O	*2.10*	3.31	3.12	3.32	2.84	2.81	3.31	*3.24*	*2.65*	*1.61*	3.05	3.22	*3.25*	3.56	*3.27*	4.04	2.22	*3.00*	3.32
K_2O	*0.32*	0.74	0.65	0.65	0.47	0.68	0.62	*0.64*	*0.40*	*0.27*	0.59	0.65	*0.64*	0.73	*0.67*	0.88	0.38	*0.63*	0.64
SrO	*0.28*	0.34	0.02	0.29	0.04	0.15	0.14	*0.04*	*0.00*	*0.17*	0.22	0.26	*0.17*	0.17	*0.24*	0.31	0.10	*0.17*	0.16
BaO	*0.05*	0.07	0.10	0.11	0.10	0.04	0.08	*0.07*	*0.04*	*0.05*	0.06	0.16	*0.08*	0.08	*0.06*	0.13	0.07	*0.05*	0.07
SUM	100.58	100.58	100.94	101.34	100.97	100.84	100.96	100.12	100.74	101.15	100.30	101.28	100.62	100.46	101.00	100.88	101.23	101.06	101.03
An	**78.8**	**65.2**	**67.3**	**65.9**	**71.6**	**70.5**	**66.7**	**66.6**	**74.0**	**83.8**	**68.9**	**66.6**	**66.1**	**63.6**	**65.8**	**58.4**	**77.5**	**68.9**	**66.6**
Ab	19.1	30.1	28.5	29.8	25.3	25.3	29.4	29.3	23.6	14.4	27.4	28.9	29.7	31.8	29.9	36.0	20.0	27.2	29.4
Or	1.9	4.4	3.9	3.8	2.8	4.0	3.6	3.8	2.3	1.6	3.5	3.8	3.9	4.3	4.0	5.2	2.2	3.8	3.7
Cs	0.2	0.3	0.4	0.4	0.4	0.1	0.3	0.3	0.1	0.2	0.2	0.6	0.3	0.3	0.2	0.5	0.3	0.2	0.3